Study of liquid metal MHD flows using OpenFOAM

Achyut Panchal
09D01002

AE 494:BTP Stage 2
Dept. Of Aerospace Engineering, IIT Bombay

Under the guidance of
Prof. Kowsik Bodi

Certificate

Certified that this B.Tech. Project Report titled "Study of liquid metal MHD flows using OpenFOAM" by "Achyut Panchal" is approved by me for submission. Certified further that, to the best of my knowledge, the report represents work carried out by the student.

Date:

Signature and name of guide : Prof. Kowsik Bodi

Acknowledgement

I would like to thank my guide Prof. Kowsik Bodi for introducing me to such an interesting subject and guiding and supporting me though out the project. I would also like to thank Prof. Shivasubramanian Gopalakrishnan, who has helped me a lot in understanding how OpenFOAM works. Finally I would like to thank Mr. Bernhard Gschaider, a developer of swakFoam, who has helped me by answering my questions on OpenFOAM forums, as early as possible. The project has been a great learning experience for me, I have gained knowledge related to magnetohydrodynamics, numerical methods and OpenFOAM.

Abstract

For the purpose of studying liquid metal MHD flows using numerical methods, it is to be validated in parts. In the present study, OpenFOAM CFD toolbox is used to apply numerical methods. The problem is partitioned in 3 parts, and separate analyses are to be done. In the present report, code validations for natural convection, 2D and 3D Magnetohydrodynamics duct flows are presented. In the end a typical natural convection case is simulated and results are compared with an experimental BARC result.
Keywords: Magnetohydrodynamics, Forced Convection, OpenFOAM, Computational fluid dynamics, Natural convection.

List of Symbols and Notations used

Re_D = Reynolds number along width
Re_L = Reynolds number along length
Cf_x = Coefficient of friction
Nu_x = Nusselt number
Gr = Grashoff number
μ = Dynamic Viscocity
ν = Kinematic Viscocity
B = Magnetic Field
σ = Electrical Conductivity
p = Pressure
CFL = Courant number
u = Velocity along length
v = Velocity along width
j = Current density
I = Current
Ha = Hartmann number
ϕ = Electrical potential
T = Temperature
β = Thermal Expansion Coefficient
Pr = Prandtl number
t = Time
g = Gravitational acceleration

Contents

1 Introduction

1.1 Motivation

Fusion energy is a source of inexhaustible energy with few of environmental drawbacks. Controlled fusion energy can clearly be a replacement for fossil fuels.[5][8]
In fusion reactions nuclei of light elements join to form heavier elements releasing enormous quantities of energy. Nuclear fusion powers the sun and other stars and is responsible for creating all the elements of the periodic table out of the primordial soup of protons and neutrons. Uncontrolled fusion is seen in case of hydrogen bomb, but it is not useful for generating power. Controlled fusion can generate desired power has proved to be very difficult to achieve practically.
These reactions are done at very high temperatures, where plasmas have to be confined by magnetic field. When a magnetic field is applied on this setup, charged particles moving at high speed will get affected by Lorentz force, and their motion can be achieved in a way so that their collisions with the wall can be reduced.
In order to cool the walls, a coolant is flowed in U shaped pipes. Pressurized helium and liquid lithium are used as coolant, liquid lithium also works as a tritium generator, since high energy neutrons will hit this lithium.
Flow in this blanket will be a major factor in deciding formation of tritium. This flow will be affected by magnetic field, heat transfer, gravity and viscous forces. This flow can be understood as MHD with forced and natural heat convection.
CFD codes are needed to take into account such fluid interactions, and models must include temperature and magnetic field couplings; in turn, the analysed system must be limited to a simplified blanket module for computational constrains.

1.2 Summary of previous work

In the previous stage of this project, simulations were done for forced convection, and 2D MHD flows. Results for fully developed velocity profiles, and entrance lengths were compared to theoretical results. Many OpenFOAM features were explored during the previous work, which are explored more in the current stage.

1.3 Progress in this report

Forced convection results are available, but natural convection was not possible in the previous stage. In this stage natural convection cases such as square cavity and open pipe are explored, and simulations are done.
As it was clear from last stage that the current method being used in OpenFOAM for MHD simulations has some flaws, such as low convergence, difficulty in 3D boundary conditions etc. The new algorithm is implemented in OpenFOAM and results are generated for both 2D and 3D flows, for various hartmann numbers.
Forced convection results were attained for a theoretical case, but it was never compared with experimental results for liquid metal in the last stage. Using a BARC experimental study, simulations are done, and results are compared with theie experimental results for validation.

2 Natural Convection

In the previous stage forced convection results were available but, natural convection results were not there. In most of the HCLL blankets, natural convection plays a major role in setting up the flow. Hot wall of the pipes will pull up the liquid metal flow.
For natural convection, available analytical results are for square cavity and open pipe. For both of these cases simulation results are compared to theoretical results[3].

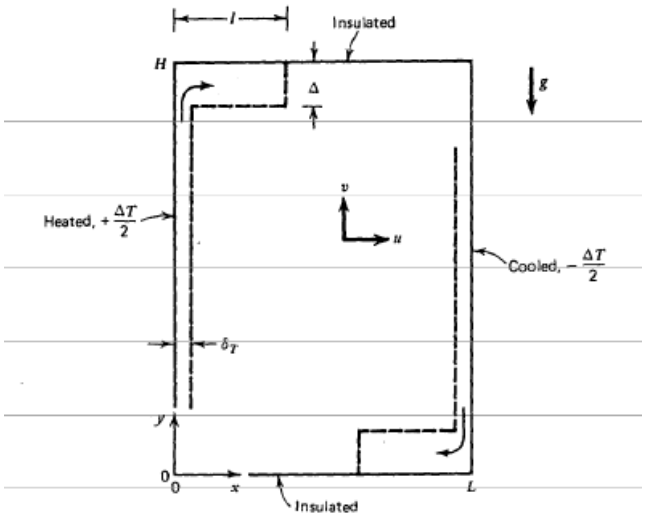

Figure 2.1: Natural convection square cavity

The first case is for a square cavity. As shown in figure 2.1, one vertical wall is heated and opposite vertical wall is cooled. It is expected that flow will start rotating inside cavity.

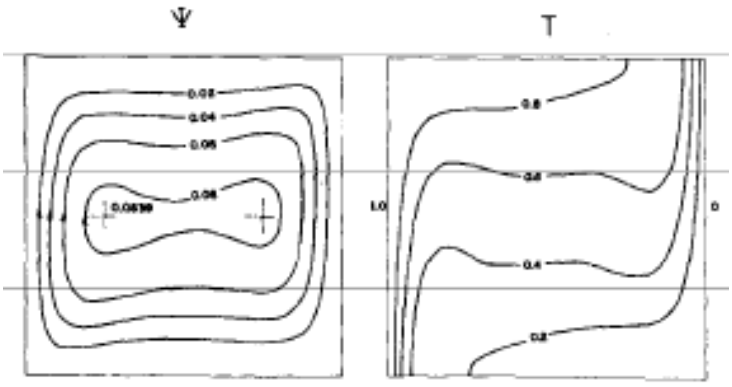

Figure 2.2: Natural convection square cavity , stream lines and isotherms

Figure 2.2 shows theoretical results of flow velocity stream lines, and isotherms. From the velocity stream lines we can say that, indeed the flow is rotating.

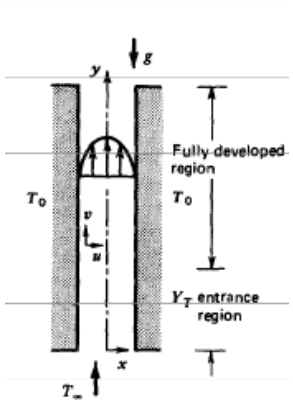

Figure 2.3: Natural convection pipe flow sucked

Another important case to validate the solver is when a hot (higher temperature then atmosphere) pipe is present above some fluid. One can say that due to this high temperature, density will decrease and, buoyancy force will cause the fluid to move upwards.
As we can see in figure 2.3, a velocity profile will be generated[3], and the flow will be sucked inside the pipe.

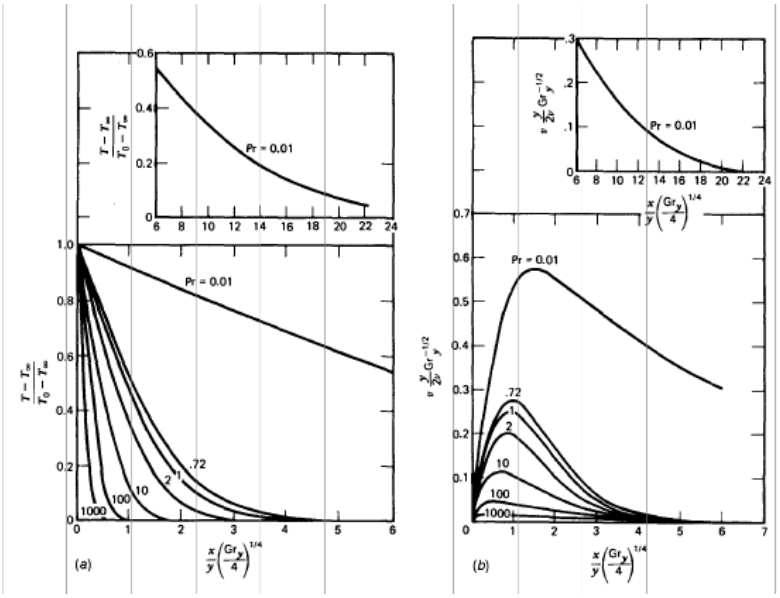

Figure 2.4: Natural convection infinite plate case

One more very important case remains, that is when one wall is hot and another wall is at atmospheric temperature, in an open pipe. This case is very much similar to what we see in HCLL blanket. In HCLL blanket also one wall will be hot, another will be cold and liquid metal flow will be sucked from tank. As the figure 2.4 shows, there are theoretical results available, for this kind of case.
However there is one problem attached with this results. They are available for cases when the cold (atmospheric temperature) wall is at infinite distance from the hot wall. During simulations it is taken care of that, this does not affect the validation drastically.

2.1 Case details

As discussed previously simulations are done for three different type of configurations in order to get a complete picture.
For the case of cavity, simulations are 2 dimensional. One wall is at 305 K and another at 295 K. Atmospheric temperature is considered to be 300 K. It is ensured that the flow remains laminar. For

this case, prandtl number (Pr) is taken as 0.71. Thermal expansion coefficient (β) is 3e-03 and laminar viscocity (ν) is 4e-04. Gravitational acceleration (g) is 9.81.
Length and width of the cavity is taken as 1 m.
Most of these typical case parameters are chosen based on availability of theoretical results to compare with.
Second case is when flow is sucked in a pipe with hot walls. Atmospheric temperature is taken as 300 K. And wall temperature of pipe is 310 K. It is ensured that the flow remains laminar. For this case, prandtl number (Pr) is taken as 0.01. Thermal expansion coefficient (β) is 3e-03 and laminar viscocity (ν) is 9.69e-07. Gravitational acceleration (g) is 9.81.
Width of the pipe is taken 0.001 m and length is taken 0.02 m.
It should be noted that, in order to get near to liquid metal properties[7], and to keep the flow laminar, the length and width have to be decreased and their values seem a little bit unrealistic.
Third and a very important case is when one wall is heated and another wall is at atmospheric temperature. Here one needs to compare with theoretical results, where distance between walls is infinite. In simulations we need to keep a finite distance, and computational time also has to be taken care of. The following figure 2.5 suggests limits for fully developed (i.e. walls very close) and flat plate (i.e. walls at infinite distance)[6].

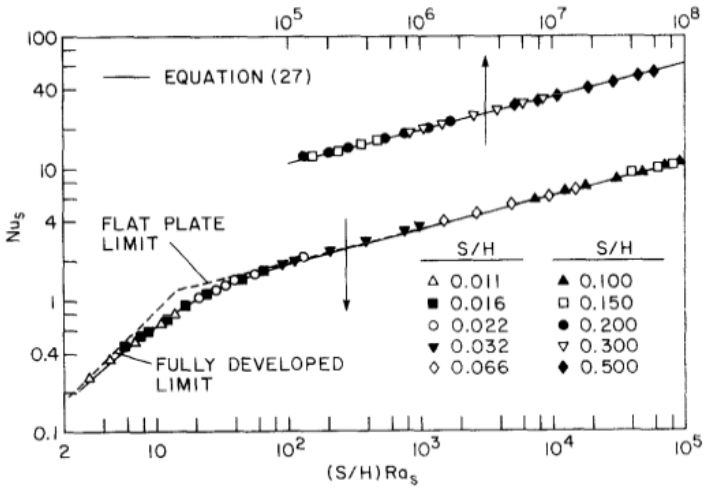

Figure 2.5: Natural convection flat plate and fully developed limits

It has been ensured that the flow remains in the flat plate region. Here also, one wall is at 310 k and atmosphere is considered to be at 300 K. Properties are same as in the above case.
length and width of the pipe is taken as 0.01 m.

2.2 Numerical method

Pressure implicit four step projection method is used for computation. textbfbuoyantBoussinesqSimpleFoam of OpenFOAM is used the first cavity case. This solver solves for U, T and p_rgh (buoyant pressure). p_{rgh} is defined as:

$$p_{rgh} = p + \rho_k g x$$

As the name of solver suggests this method makes use of boussinesq approximation. Density can be assumed constant in all the equations, accept the buoyancy force term. rho_k is defined as following.

$$\rho_k = 1 - \beta(T - T_{ref})$$

Boundary conditions are also to be given in terms of p_rgh. This feature works very well for the

case of cavity. But in the case of an open pipe when p is constant, not p_rgh, this formulation starts creating problems.
In order to deal with such a problem. Some changes are dont in the solver. The solver is reformulated to solve the p equation, instead of p_rgh equation. In the new solver, the algorithm or numerical methids are not changed.
Later it was realized that same thing can also be done by an extension to OpenFOAM, known as groovyBC. By using both the methods, results were generated and valodated.

2.3 Results

2.3.1 Square cavity

The simulation results of laminar, steady state square cavity case are presented.

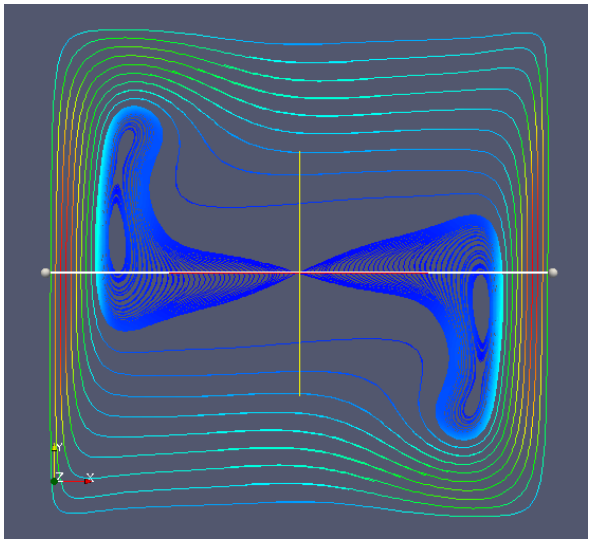

Figure 2.6: Natural convection square cavity velocity stream line simulation result

The above figure 2.6 is very much similar to the theoretical velocity stream line plot in case of a square cavity. The colour code represents magnitude of velocity at that point, red being maximum and blue being minimum.
In the next two plots velocity at center line are plotted for both x and y direction. Here it shuold be noted that y is the vertical direction (i.e. g is acting along -y direction)// This profiles are theoretically available, to compare with.

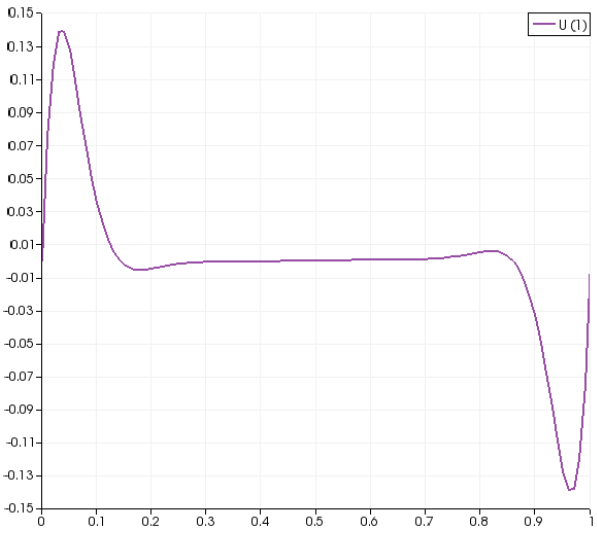

Figure 2.7: Natural convection square cavity velocity in y direction

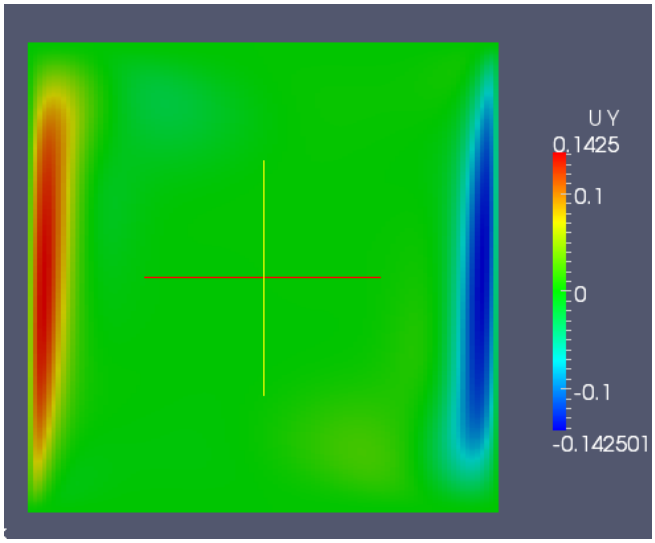

Figure 2.8: Natural convection square cavity velocity in y direction

It can be seen that the results are matching quite nicely.
In order to understand the phenomenon, it can be seen from the x and y velocity profiles, and velocity streamlines, that the flow is indeed rotating. Flow is upwards near the hot wall, and it is going down near cold wall.

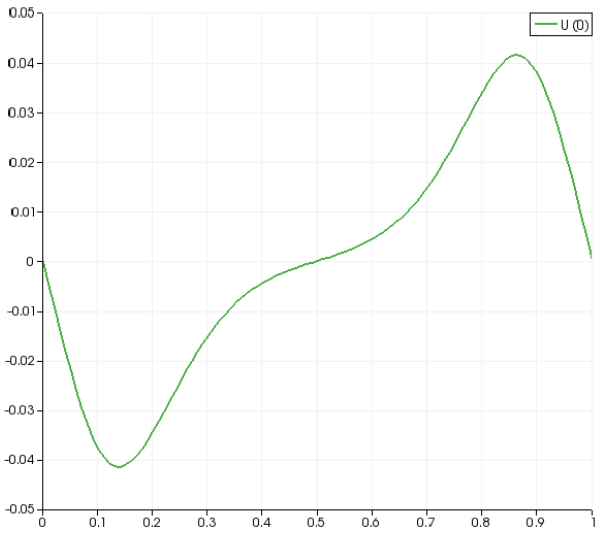

Figure 2.9: Natural convection square cavity velocity in x direction

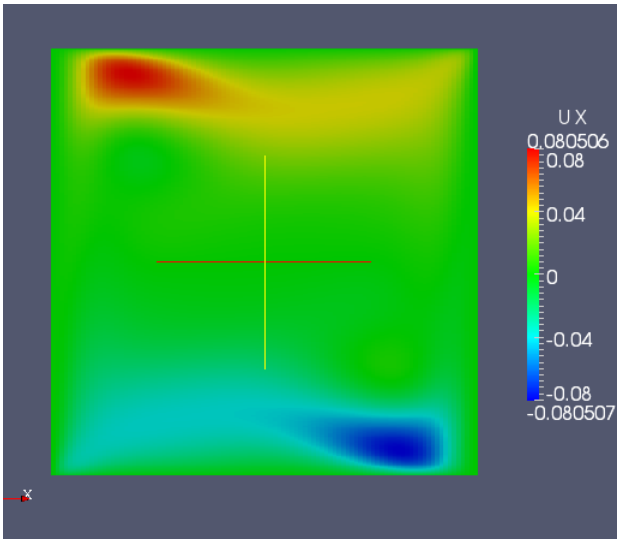

Figure 2.10: Natural convection square cavity velocity in x direction

In all the cases, blue colour represents lower value and red colour represents higher value. ALong with the effect of rotating flow due to buoyancy force, one should also take in note that, the flow is zero at wall boundaries, that is no-slip bounary condition. Due to this, viscous friction force also will be acting.

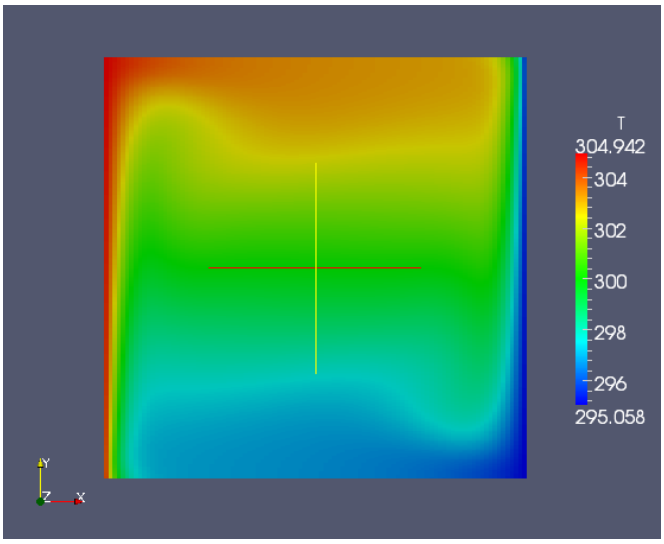

Figure 2.11: Natural convection square cavity temperature

From the temperature contours, one can see that temperature is higher on the upper parts of cavity, as compared to the lower parts.

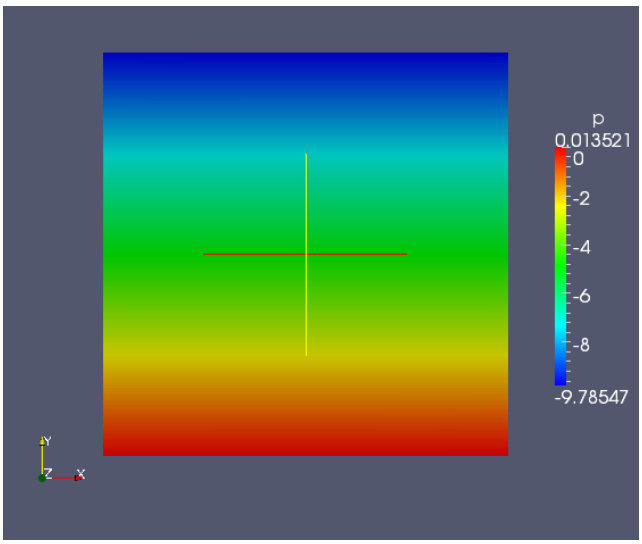

Figure 2.12: Natural convection square cavity pressure

Pressure distribution along vertical direction is linear, leading to the fact that variation in $p_r gh$ is low compared to variation in term $rho_k gh$. The slope of vertical pressure variation is almost same as g.

2.3.2 Fully developed open pipe flow

In this case the flow should be sucked upwards, and the profile should be symmetric. Following expression represents the theoretical result for velocity profile[3].

$v = \frac{g\beta D^2(T_0 - T_\infty)}{8\nu}[1 - (\frac{x}{D/2})^2]$

The velocity profile should be parabolic.The velocity is sucked by the temperature difference between wall and atmosphere. So, it should be noted that, higher the temperature difference, higher will be mass flow.

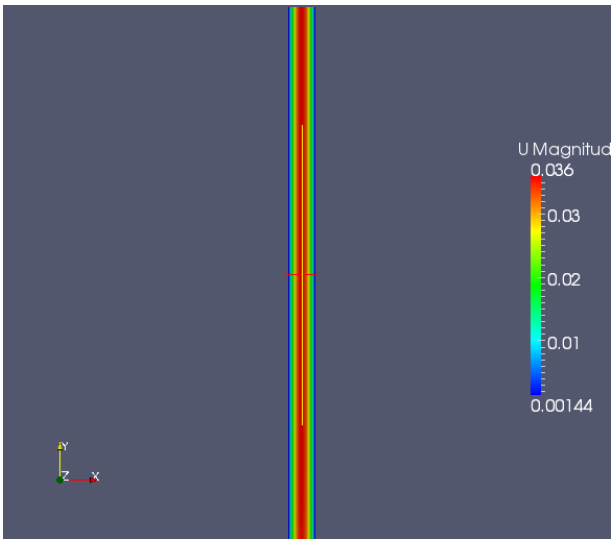

Figure 2.13: Natural convection ,pipe flow, velocity

Here pressure boundary conditions are given as if the pipe is open (i.e. pressure same as atmospheric pressure at that height) One can see that pressure varies linearly vertically with a slope of g.

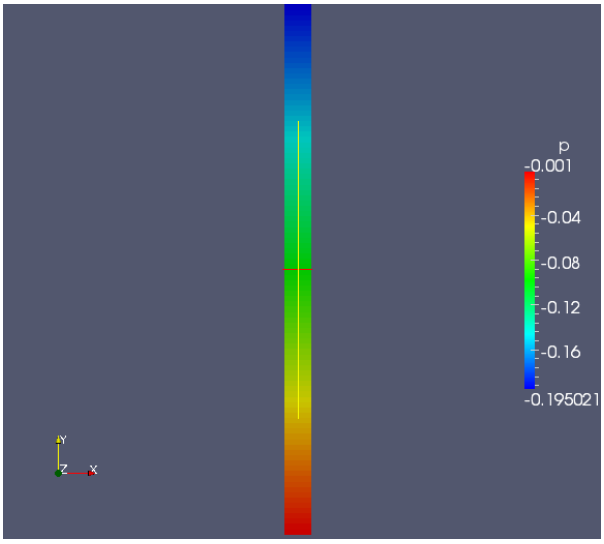

Figure 2.14: Natural convection ,pipe flow, pressure

As the heat is given to the flow not in a form of constant heat flux, but in the form of a constant higher temperature. We can see from the temperature contour figure 2.15 that, after some entrance length region temperature is quite the same as wall temperature.

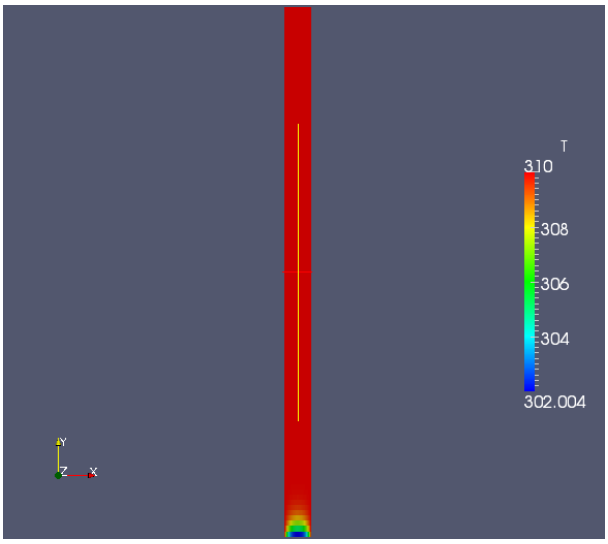

Figure 2.15: Natural convection ,pipe flow, temperature

2.3.3 Flat plate limit natural convection flow

In this case, there is a temperature difference across the walls. It is expected that due to one wall being on a higher temperature, the flow will be sucked due to buoyancy force in the pipe. ALl the simulations are for 2D, laminar, steady state.

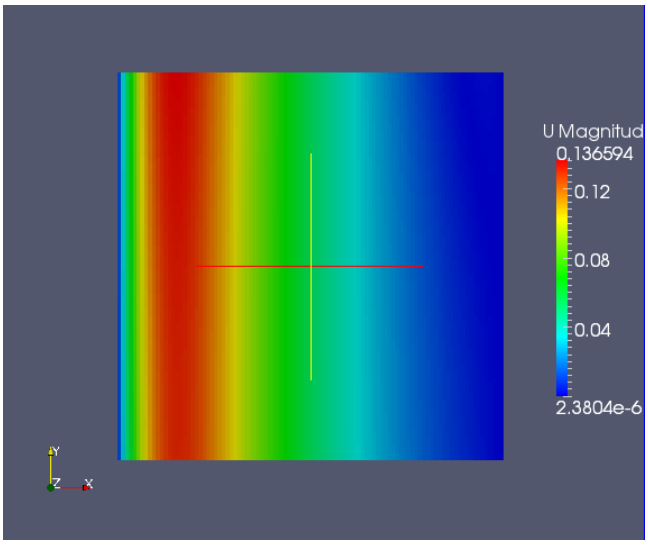

Figure 2.16: Natural convection velocity build up

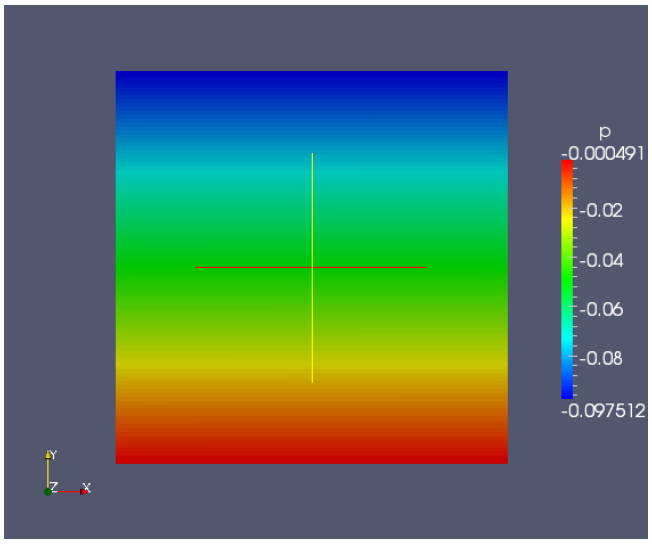

Figure 2.18: Natural convection pressure variation

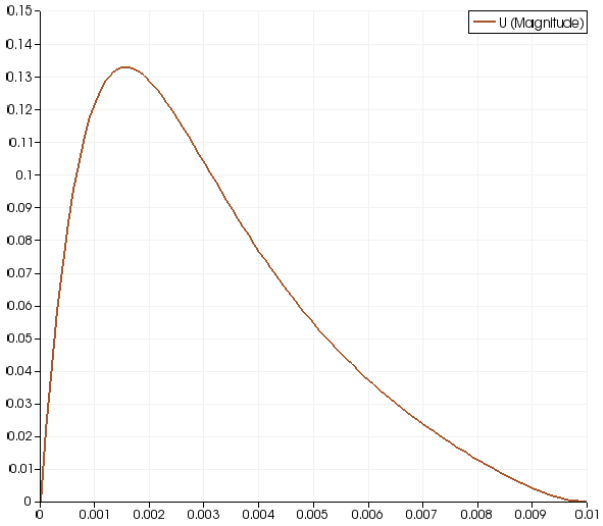

Figure 2.17: Natural convection velocity profile

It is observed that velocity is zero at the walls, due to no slip boundary condition. Velocity reaches a maximum somewhere near the hot wall.
It can be seen that since the flow is not fully developed.

Pressure variation again follows the same trend and decreases linearly in vertical direction.

It is seen that since the flow is not fully developed, the temperature profile continuously grows, and spreads in low temperature regions.

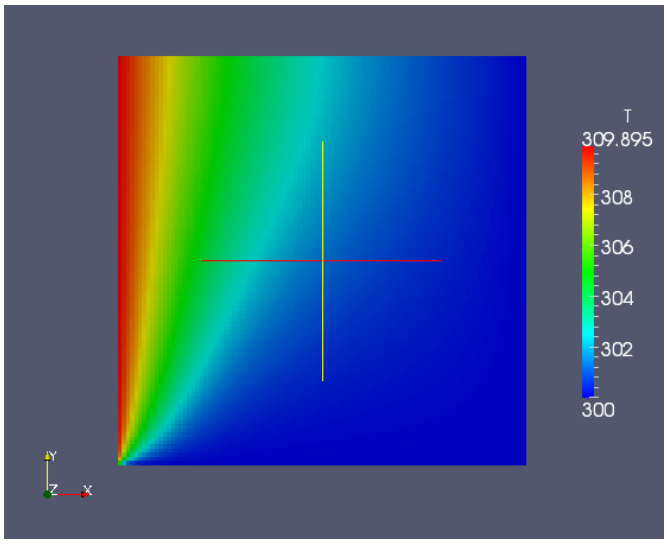

Figure 2.19: Natural convection temperature variation

3 Magnetohydrodynamics flow 2D

In the previous stage 2D magnetohydrodynamics flow simulations were done for a shercliff case[12] where walls perpendicular to magnetic field are non conducting but current can flow in the direction perpendicular to magnetic field direction. Fully developed velocity profiles are studied and compared with theoretical results.
Numerical method used in previous phase was magnetic field induction. It is seen that this method is slow in converging. For fusion reactor liquid metal simulations, usually hartmann numbers are as high as 1000[8]. At such higher hartmann numbers, there is a need of very fine grid and hence very small time step. This leads to very high computation time. And if convergence is slow then simulations become practically very much difficult.
Some sources suggest that it is difficult to give proper boundary conditions in 3D case with magnetic field induction method.
Along with the above reasons, in case of liquid metal magnetic reynolds number is vary much small. Small magnetic reynolds number leads assumption that, magnetic field remains approximately constant and induced magnetic field is zero. The above assumption leads to a new numerical method known as electric potential method. In this method electric potential equations are solved instead of induced magnetic field equations.
Using OpenFOAM tools such a solver using electric potential method was developed (attached in appendix). The same case as in previous stage was simulated again and fully developed velocity profiles were matched with theoretical results.

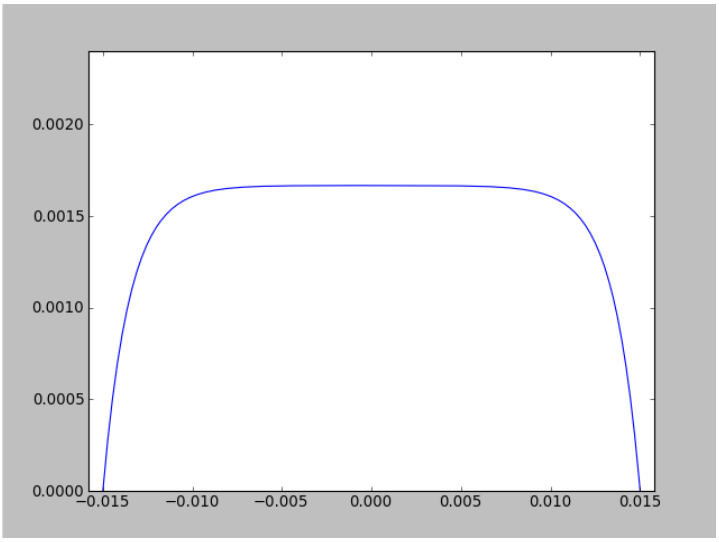

Figure 3.1: 2D MHD pipe flow velocity profile, Hartmann number 10

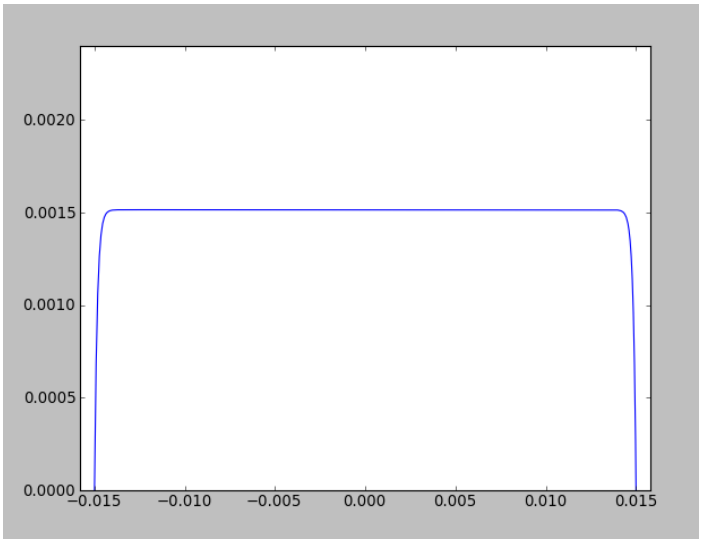

Figure 3.2: 2D MHD pipe flow velocity profile, Hartmann number 100

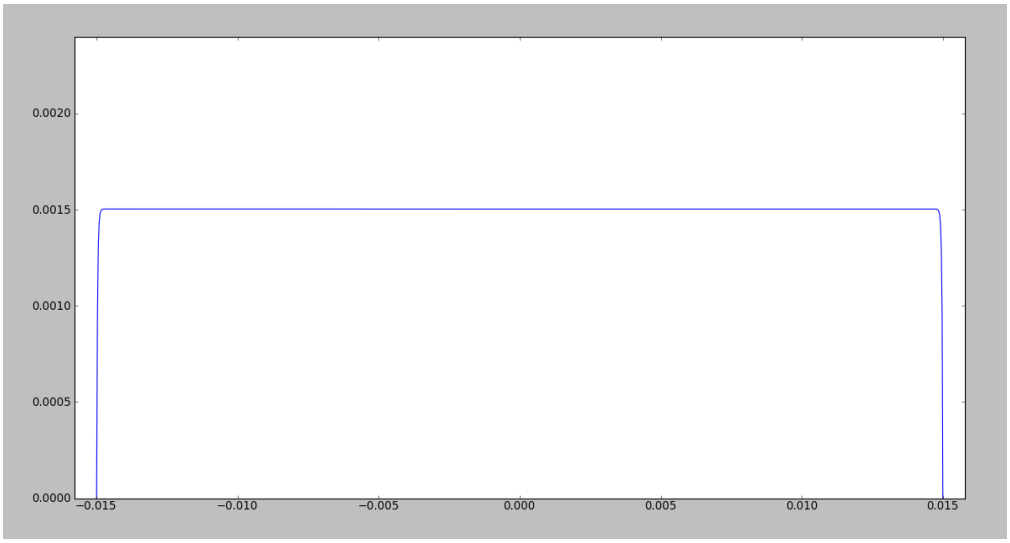

Figure 3.3: 2D MHD pipe flow velocity profile, Hartmann number 500

Figures 3.1, 3.2 and 3.3 are theoretical 2D velocity profiles for various hartmann numbers. As hartmann number is higher higher is the magnetic field. It should be noted that hartmann number represents ratio of magnetic force and viscous force. One can see from the profiles that as hartmann number increase, velocity profile gets flatter.

$Ha = BL\sqrt{\frac{\sigma}{\mu}}$

Theoretical equation for 2D MHD velocity profile is following[4]:

$u = \frac{HacoshHa}{HacoshHa - sinhHa}[1 - \frac{cosh(Hay)}{coshHa}]$

In practical situations hartmann numbers are as high as 10,000. But beyond Ha =1000, it becomes difficult to calculate theoretical solution of velocity profile due to computational aspects.

3.1 Case details

The same case that was simulated in the previous stage is simulated again using the same method. In a 2D duct inlet velocity is specified as 0.0015 m/s for all cases. Permeability (μ) is taken as 1-e06. Electrical conductivity (σ) is 8000. Pipe width is 0.03 m and length is taken as 0.18 m. Density is taken as 9926 kg/m^3. And viscocity is 3.925e-04[7]. The above properties are kept same for all the cases, and magnetic field is changed in order to change hartmann number. It has been ensured that the flow stays laminar.
As discussed above, at high hartmann numbers, boundary layers are very small, hence mesh element size near wall has to be very small. This leads to non uniform mesh. An example of such a mesh is given in the figure 3.4.

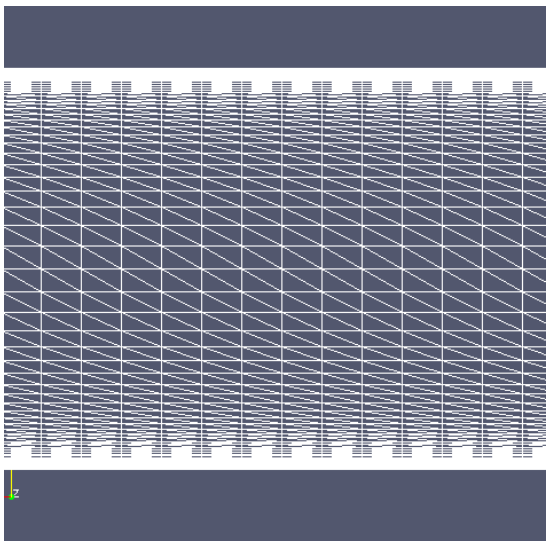

Figure 3.4: Non uniform mesh used for simulations

3.2 Numerical method

As discussed above, in this method instead of magnetic field induction, eletric potential is used.
In general electric field can be written as the following expression.

$$\vec{E} = -\nabla\phi - \frac{\partial\vec{A}}{\partial t}$$

Now since this is ressistive magnetohydrodynamics we can apply ohm's law as the in the following equation. Another assumption in the next equation is that induced magnetic field is very small.

$$\vec{j} = \sigma(-\nabla\phi + (\vec{U} \times \vec{B_0}))$$

From the conservation of electric charges we can say that

$$\nabla \cdot \vec{j} = 0$$

By combining the above equations we get the following equation, which is considered as the electric potential equation for this kind of solvers. This equation will be solved in the solver.

$$\nabla^2\phi = \nabla \cdot (\vec{U} \times \vec{B_0})$$

Now we see how boundary conditions are applied in this case. If $\vec{n}$ is vector normal to the boundary wall. Then the following condition suggests that no current is passing through that boundary, that is insulated boundary condition. This is a neumann boundary condition.

$$\frac{\partial\phi}{\partial n} = (\vec{U} \times \vec{B_0})_{boundary} \cdot \vec{n}$$

If boundary is conducting, in that case there will be a specific electric potential attached to that. So conducting wall boundary condition is given as following. This is a dirichlet boundary condition.

$$\phi = \phi_0$$

Second order four step projection methods are used in order to solve the equations. While applying this method, it has been ensured that the scheme is conservative and consistent. Fluid dynamics equations and electric potential equation is solved as if they were decoupled equations during a single time step. It was observed that at high hartmann numbers, convergence was hard for this method also. In order to fix that relaxation factors were used. As relaxation factor plays an important role here; since the method is only checked for steady state and not for transient cases, it may not give satisfactory results for transient case.

3.3 Results

In the case of high hartmann number, velocity profile will be flat. In that case, viscous forces in the core region will be minimal, but will be higher in boundary layer. In case of high hartmann number, magnetic forces also will be high.

3.3.1 Validation with theoretical profiles

In all various hartmann number cases, there are various forces affecting the steady state, so pressure variation along length also will be different for all case. In the following figures, simulation results for velocity profiles, and pressure variations along length for various hartmann numbers are plotted.

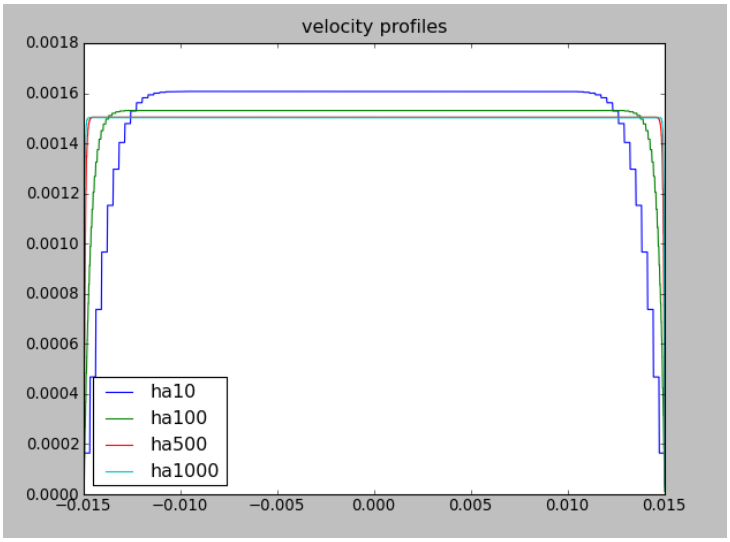

Figure 3.5: 2D MHD pipe flow simulation velocity profiles

Flow can be divided in two parts, core flow and boundary layer flow. In the core region, magnetic field will decelerate flow, and in boundary layer region, magnetic field will accelerate the flow. At high hartmann numbers, most of the flow will be in core region. In that case, higher the megnetic field (hartmann number) higher will be drag, and so higher pressure gradient along length will be required.

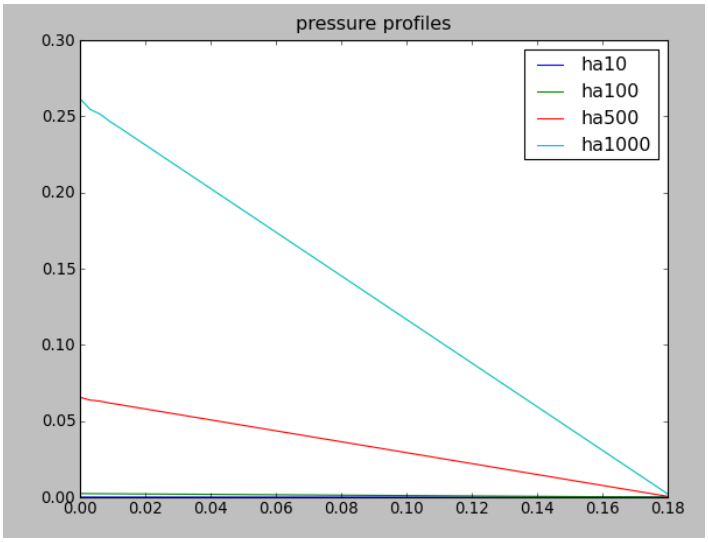

Figure 3.6: 2D MHD pipe flow simulation pressure along length

3.3.2 Boundary layer study

There are benifits of estimating boundary layer thickness[10], for MHD duct flow. One of them being that, once boundary layer thickness is known, simulations need to be done for only boundary layer, and flow in the core region can be considered constant. This will reduce computation effort by a huge amount.
Some theoretical results suggest that hartmann boundary layer is inversely proportional Hartmann number.

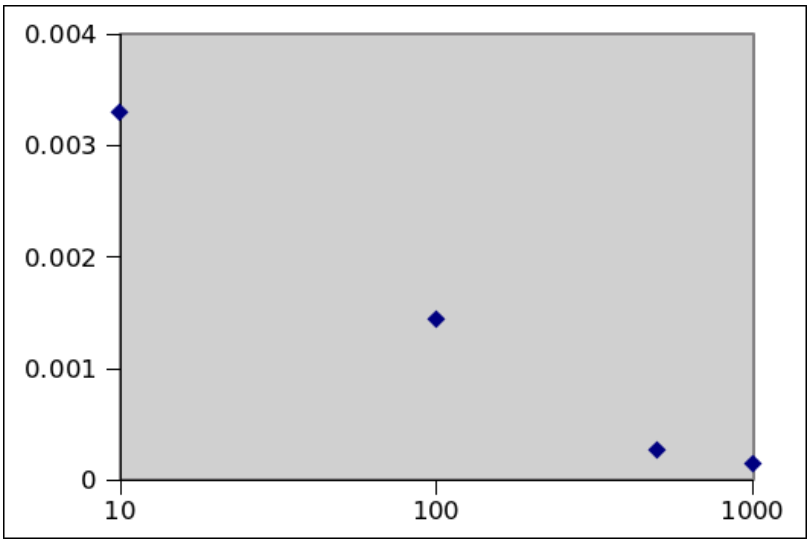

Figure 3.7: 2D MHD pipe flow simulation 0.99 % U_core boundary layer thickness

For estimating boundary layer thickness, three methods are applied.

Method 1

Boundary layer thickness can be estimated from the velocity profile. In this method, boundary layer thickness is defined as thickness, when velocity is 99% of the core velocity.

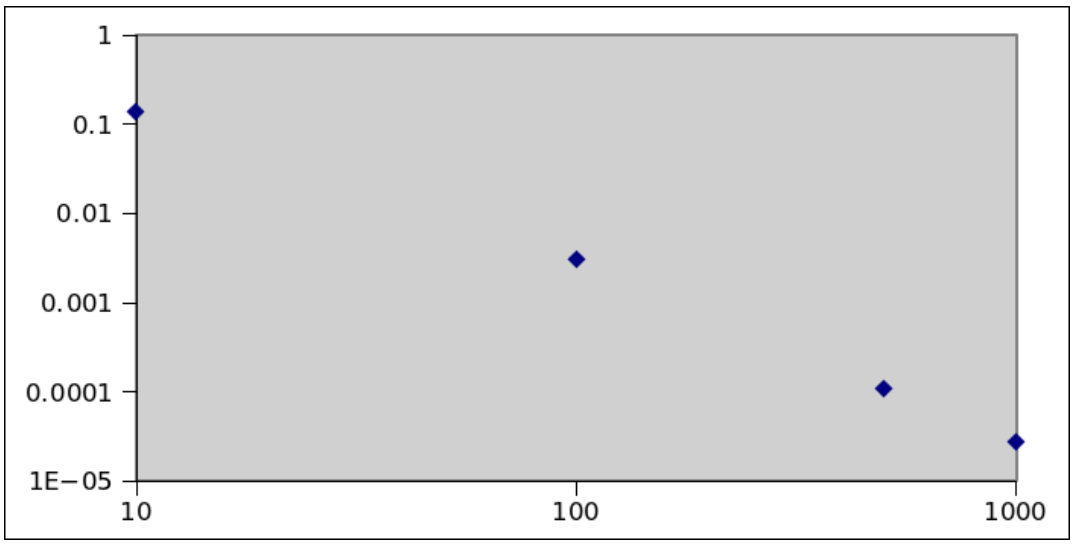

Figure 3.8: 2D MHD pipe flow simulation boundary layer thickness method 2

Method 2

For viscous flows, without any magnetic fields, boundary layer thickness is approximated by the following method.

$$\mu \frac{U_0}{\delta} = \tau_w (perimiter) L = \Delta P (Area)$$

So if pressure gradient, fluid properties, and pipe dimensions are known , boundary layer thickness δ can be estimated. Here it is assumed that no other force then pressure and viscovity is acting.
One way to calculate boundary layer thickness for our problem is directly use this formula, and since we know pressure gradient along length, we can get some numbers. Method 2 is the same thing.

Method 3

However one can argue that since in case of MHD, pressure and viscous force are not the only two forces, this formulation might not help. So, we assume the following.
For high hartmann numbers, most of the flow is outside boundary layer. In this region we can assume

that magnetic field is applying a force in the opposite direction of flow. So, we can say that pressure gradient is balanced by shear force and magnetic force ($j \times B$). Assuming j to be constant in the whole region.

$j = \sigma(U \times B)$

We can compute boundary layer forces $\tau_w(perimiter)L$ by applying force equilibrium.

$\tau_w(perimiter)L = \Delta P(Area) - j \times B$

Now with this value of $\tau_w(perimiter)L$ we can get boundary layer thickness δ.

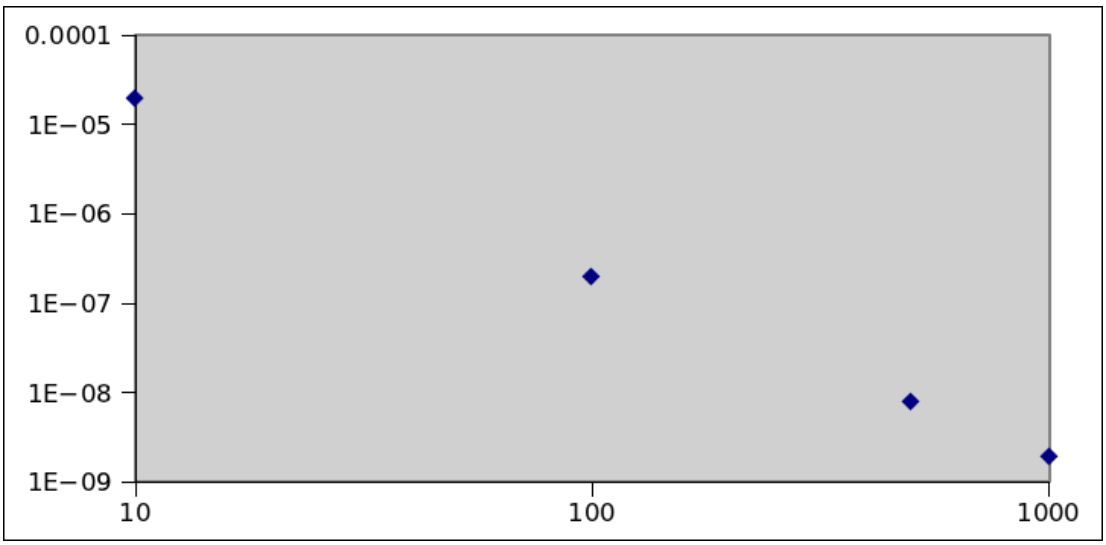

Figure 3.9: 2D MHD pipe flow simulation boundary layer thickness method 3

This boundary layer thickness are calculated from simulated results for various hartmann numbers. These results are plotted with hartmann numbers. It can be seen that logarithmic plots are linear between boundary layer thickness and hartmann number.
It should be noted that unlike method 2 and method 3, in method 1 plots, boundary thickness axis is not in logarithmic scale. Although methods are different for calculation of boundary layer thickness, all the methods give similar trend with varying hartmann number.

4 Magnetohydrodynamics flow 3D

In the previous section it was seen that the results are quite satisfactory for the 2D case. A major benifit we should get from using electric potential method is being able to run for 3D cases.
We will be solving for a 3D square cross section pipe. For 3D magnetohydrodynamic flows there are 2 theoretical results available, known as hunt's case[9] and shercliff case[12]. Shercliff case is when all the walls are non conducting. Hunt case is when walls can be either conductive or non conductive.
Shercliff case can be better understood seing the figure 4.1.

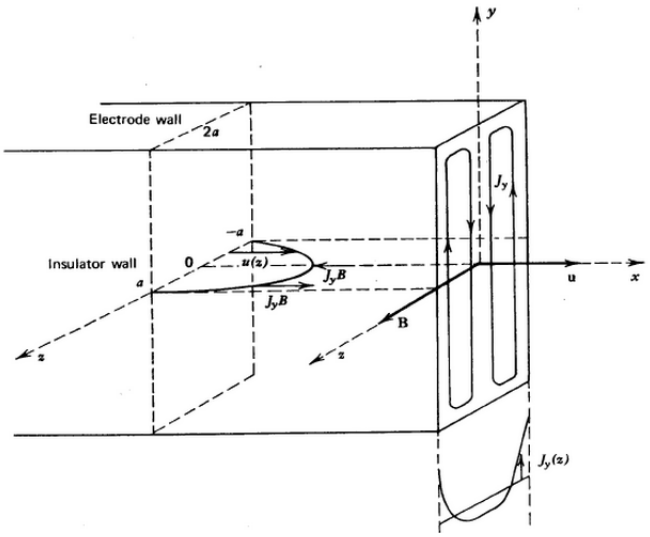

Figure 4.1: Shercliff case

In this case all the walls are non conducting. Magnetic field is applied perpendicular to one set of walls and parallel to another set of walls. Since the walls are non conducting, and there cannot be any current sources or sinks, current flows in a loop as shown in the figure. This leads to the fact that, magnetic force accelerates flow in boundary layer region and it decelerates flow in the core region[4], hence the flat profile.
For any this kind of case, there wil be two different velocity profiles generated, one parallel to magnetic field, and another perpendicular to magnetic field. The one which is parallel to magnetic field is known as hartmann layer, and another is known as side layer.
It is observed that for high hartmann numbers, hartmann profile is same as 2D case.
As it was for the 2D case, here also, as hartmann number and hence magnetic field is increased, the velocity profiles get flatter and flatter.
Shercliff theoretical solution is available as an infinite series[12]. A matlab code available was used in order to generate profiles. Profiles are generated for hartmann layer, and side layer at various positions. For hartmann number 0, the case is same as viscous flow in a square duct. It is observed that, maximum velocity is obtained at center, and it is double the uniform inlet velocity. In case of Hartmann number zero, both the profiles, hartmann layer and side layer are same.

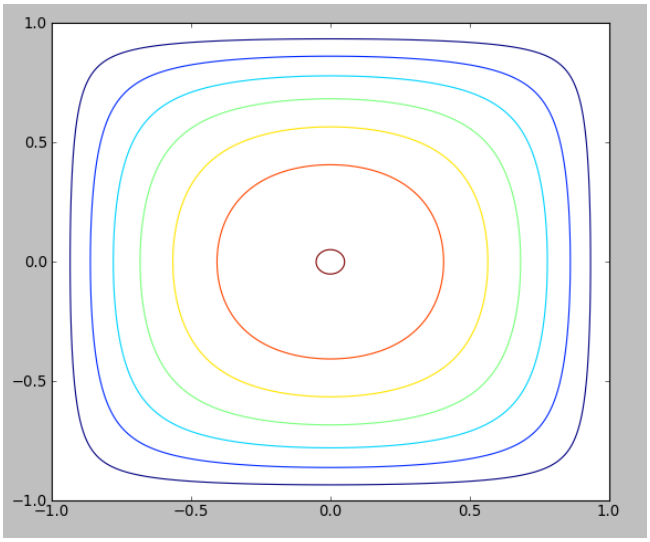

Figure 4.2: 3D analytical MHD pipe flow velocity contour, Hartmann number 0

In the contours, red colour represents high velocity and blue represents low velocity.

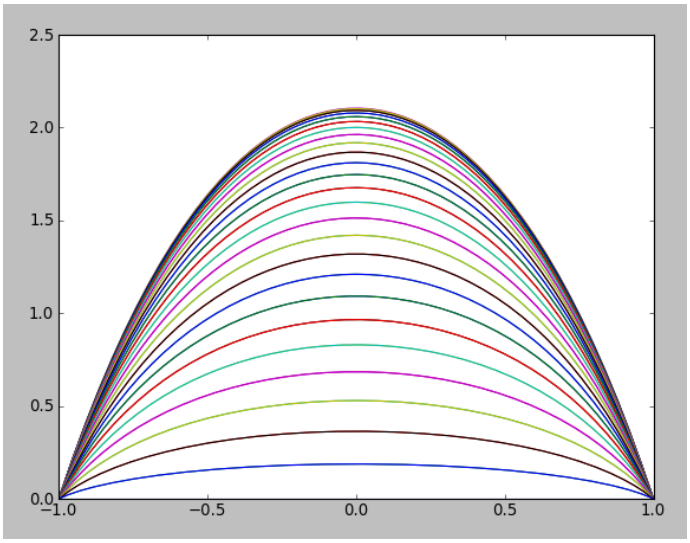

Figure 4.3: 3D analytical MHD pipe flow velocity sidelayer, Hartmann number 0

Different coloured lines represents velocity profiles at various locations. The one which has maximum velocity higher compared to all the other profiles, is the center velocity profile.

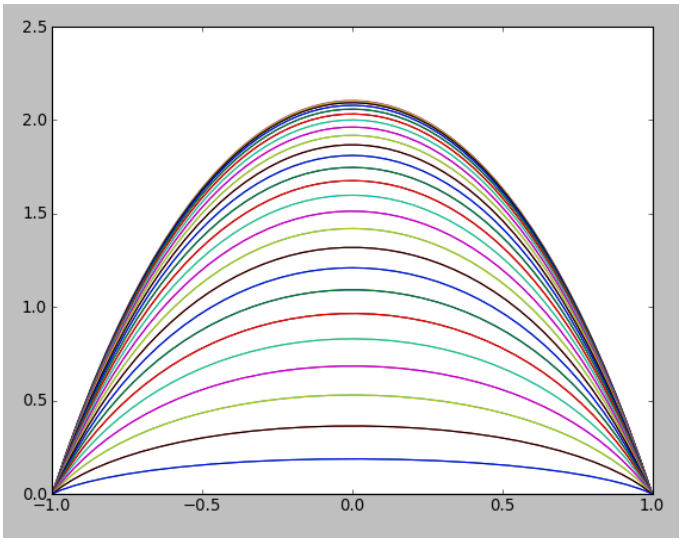

Figure 4.4: 3D analytical MHD pipe flow velocity hartmann layer, Hartmann number 0

For hartmann number 10, as it was expected, profile becomes flatter.

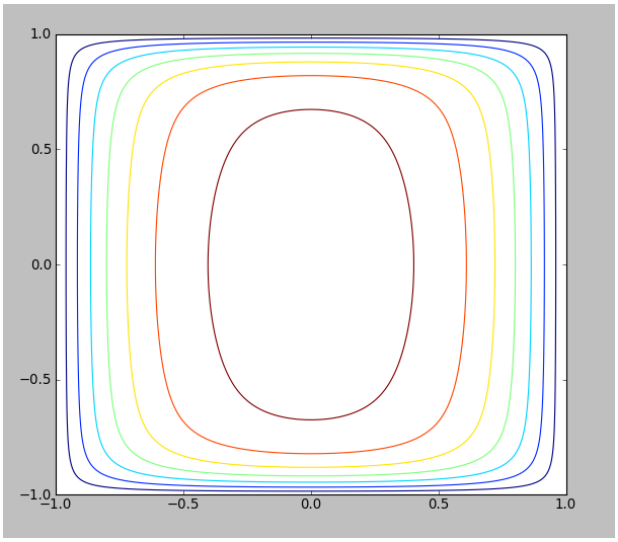

Figure 4.5: 3D analytical MHD pipe flow velocity contour, Hartmann number 10

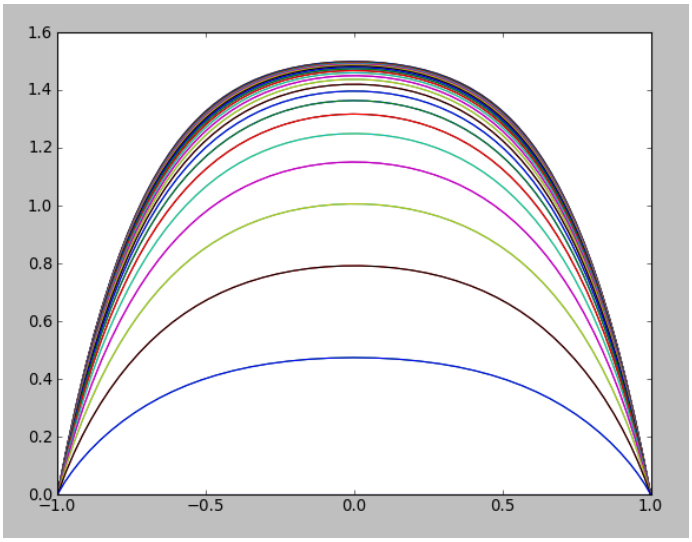

Figure 4.6: 3D analytical MHD pipe flow velocity sidelayer, Hartmann number 10

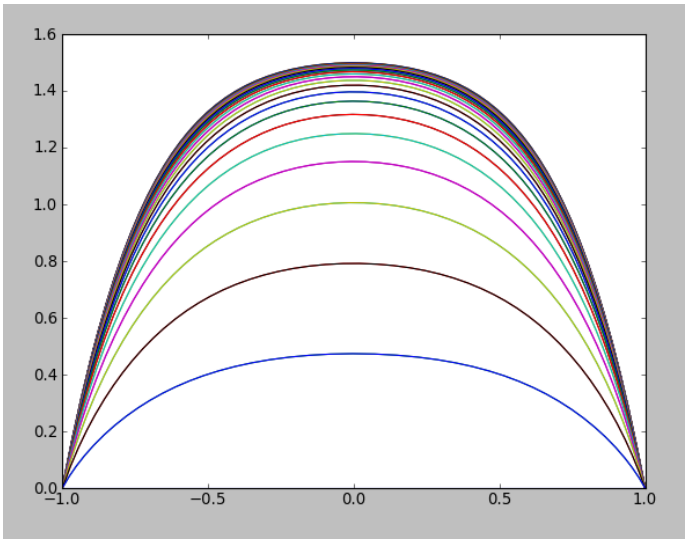

Figure 4.7: 3D analytical MHD pipe flow velocity hartmann layer, Hartmann number 10

For high hartmann numbers, hartmann layer velocity profiles are very much similar to 2D case velocity profiles.

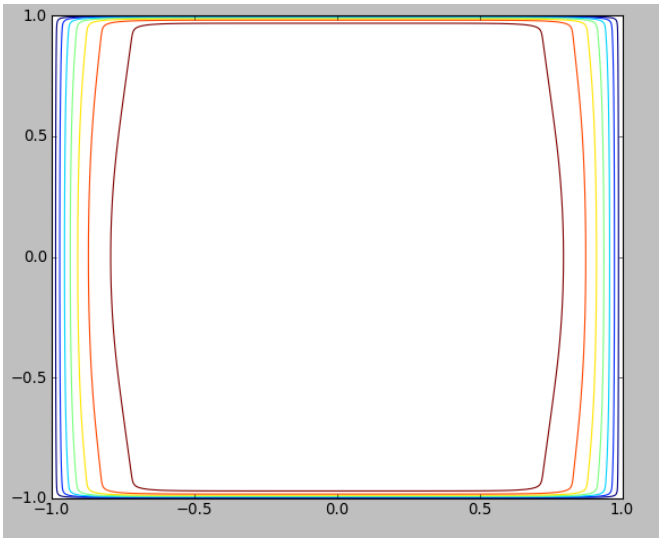

Figure 4.8: 3D analytical MHD pipe flow velocity contour, Hartmann number 100

From velocity contours also, it can be observed how profile is getting flatter, and boundary layer velocity variation is getting steep.

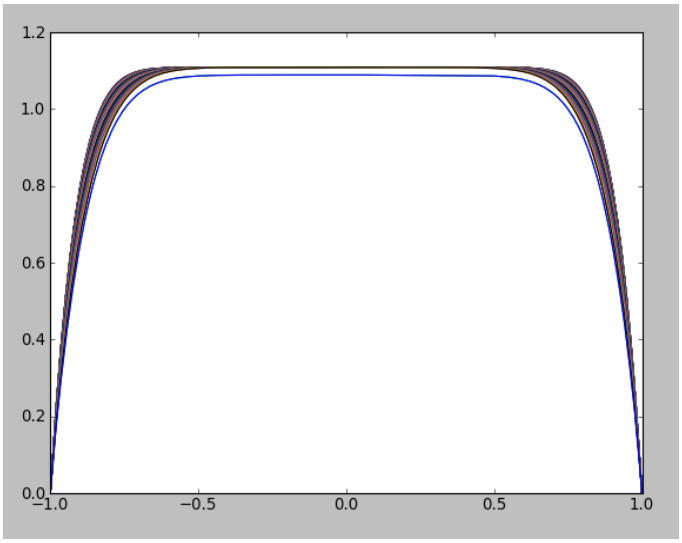

Figure 4.9: 3D analytical MHD pipe flow velocity sidelayer, Hartmann number 100

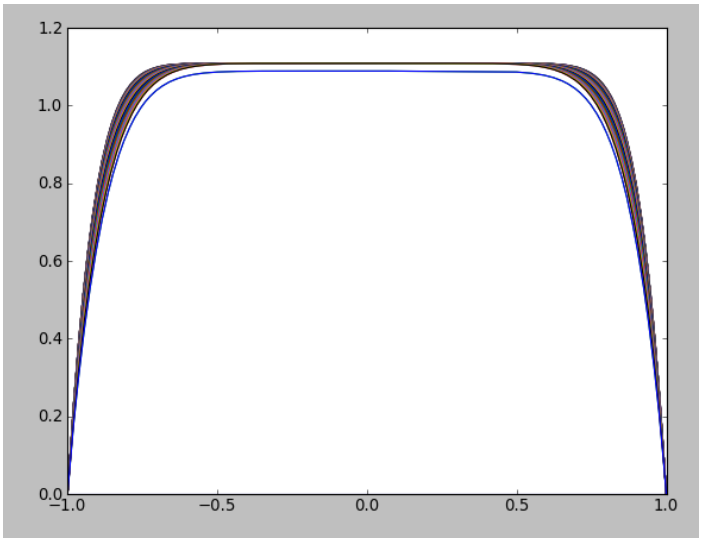

Figure 4.10: 3D analytical MHD pipe flow velocity hartmann layer, Hartmann number 100

Difference between hartmann layer and side layer is easily observed by looking at contour profiles. Some researchers have suggested that, hartmann layer boundary thickness is proportional to $1/Ha$ and side layer boundary thickness is proportional to $1/Ha^{\frac{1}{2}}$. So the one with steep change in velocity is hartmann layer thickness. In the current contour figures, vertical direction is hartmann layer.

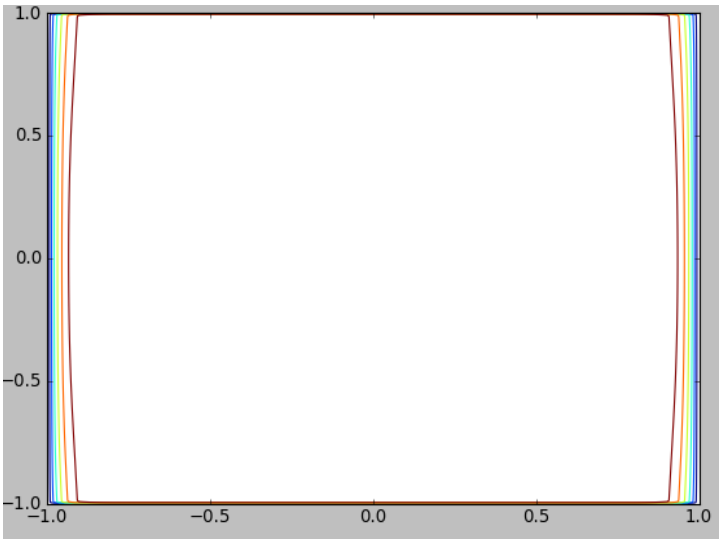

Figure 4.11: 3D analytical MHD pipe flow velocity contour, Hartmann number 500

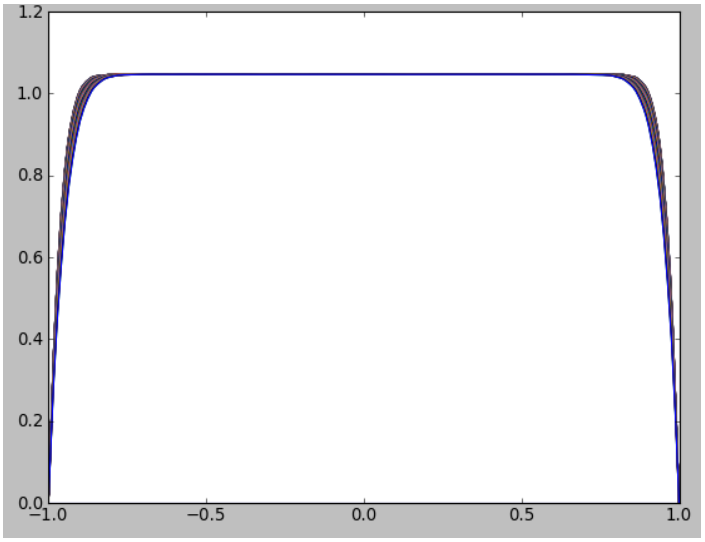

Figure 4.12: 3D analytical MHD pipe flow velocity sidelayer, Hartmann number 500

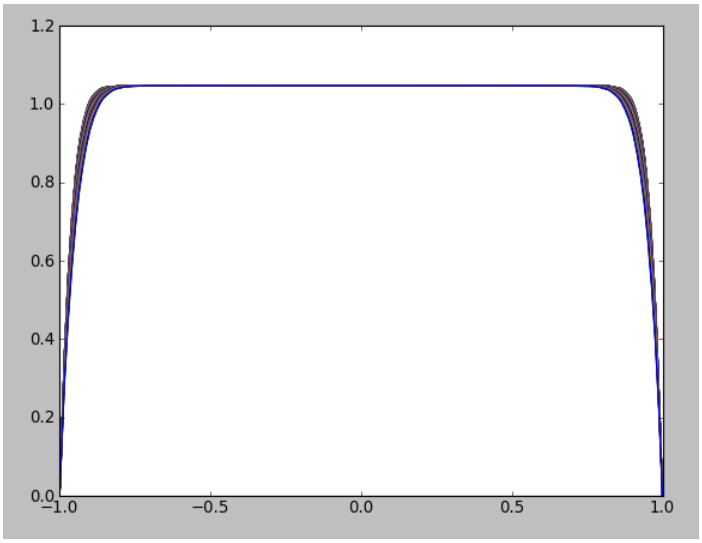

Figure 4.13: 3D analytical MHD pipe flow velocity hartmann layer, Hartmann number 500

4.1 Case details

A square cross sectioned pipe is used for the simulations. In a 3D square duct inlet velocity is specified as 0.0015 m/s for all cases. Permeability (μ) is taken as 1-e06. Electrical conductivity (σ) is 8000. Pipe width and height are 0.03 m and length is taken as 0.18 m. Density is taken as 9926 kg/m^3. And viscocity is 3.925e-04[7]. The above properties are kept same for all the cases, and magnetic field is changed in order to change hartmann number. It has been ensured that the flow stays laminar.
At high hartmann numbers as in the previous cases, boundary layer is very thin. In order to capture that highly non uniform mesh elements are use. Especially at corners mesh elements are very small.

4.2 Numerical method

As the mesh is non uniform for this 3D case, it becomes necessary to check for conservation and consistence. OpenFOAM epot solver is used as was used for 2D cases.
Since all the walls are non conducting, electric potential is given zero normal gradient boundary condition at walls. Along with that, no slip condition is given for velocity at boundaries.
Along with velocity side layer and hartmann layer profile. Current stream lines are also observed.

Current stream lines near corners gives an idea about whether methid is conservative or not.

4.3 Results

Results are presented for various hartmann number flows simulated. Folliwing are the figures for hartmann number 10. It can be onserved that, velocity is maximum in the center region. In the starting region, flow is developing so there is some disturbance, which gets cleared up as the flow developes. Velocity profile along hartmann layer and side layer also can be seen. They both are qualitatively similar. However one can clearly notice that boundary layer for hartmann is thinner compared to side layer. Next graph represents current stream lines. It is important to note that since walls are non conducting, and there are no curren sources or sinks in the pipe, the current lines will make loops as in the figure 4.1. The fact that current lines are not going normal in to the wall, shows that scheme is conservative in the non uniform mesh region.
Results can be compared with analytical results for shercliff problem.

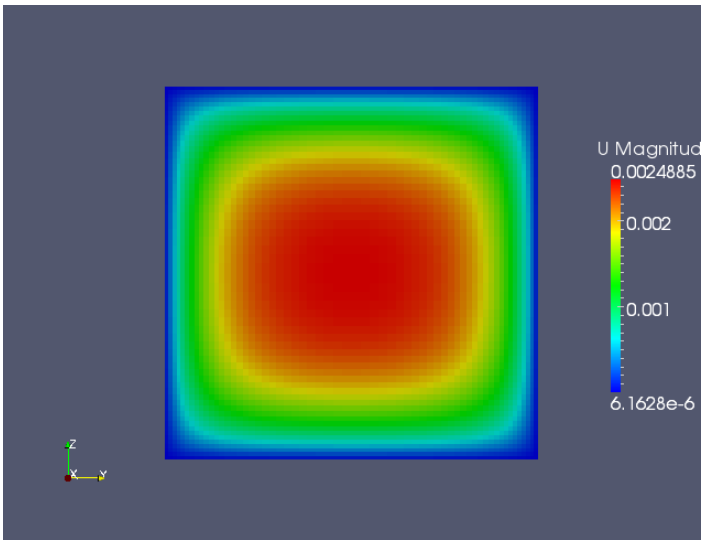

Figure 4.14: 3D MHD pipe flow simulation velocity contour Hartmann number 10

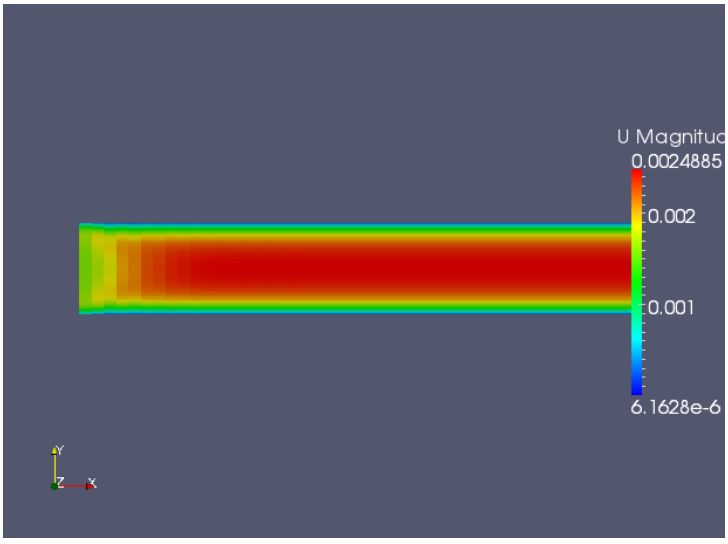

Figure 4.15: 3D MHD pipe flow simulation hartmann layer velocity Hartmann number 10

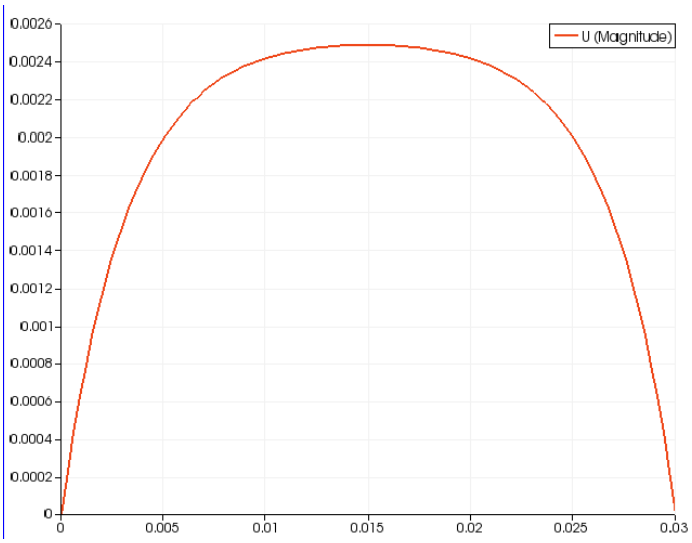

Figure 4.16: 3D MHD pipe flow simulation hartmann layer velocity profile Hartmann number 10

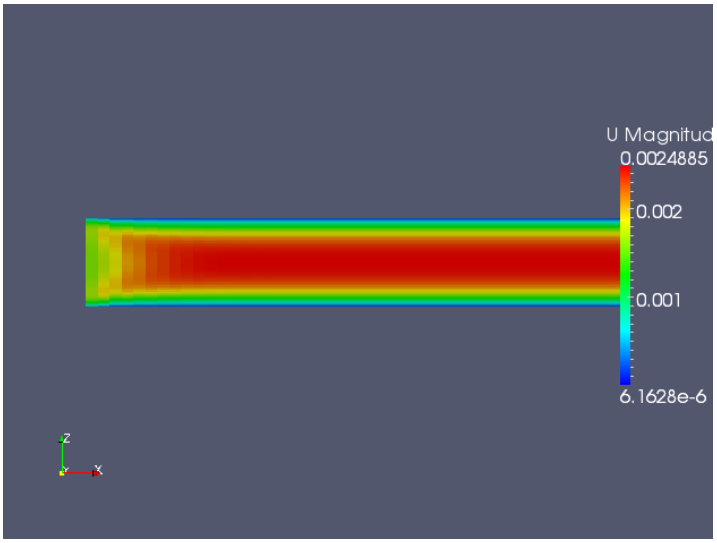

Figure 4.17: 3D MHD pipe flow simulation side layer velocity Hartmann number 10

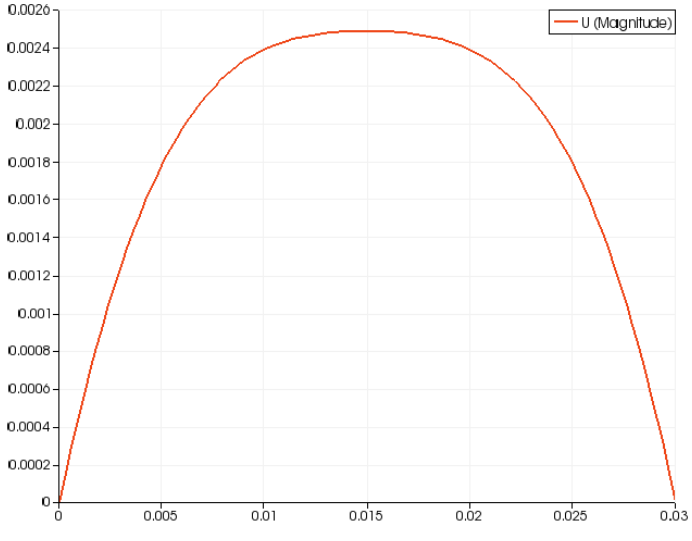

Figure 4.18: 3D MHD pipe flow simulation side layer velocity profile Hartmann number 10

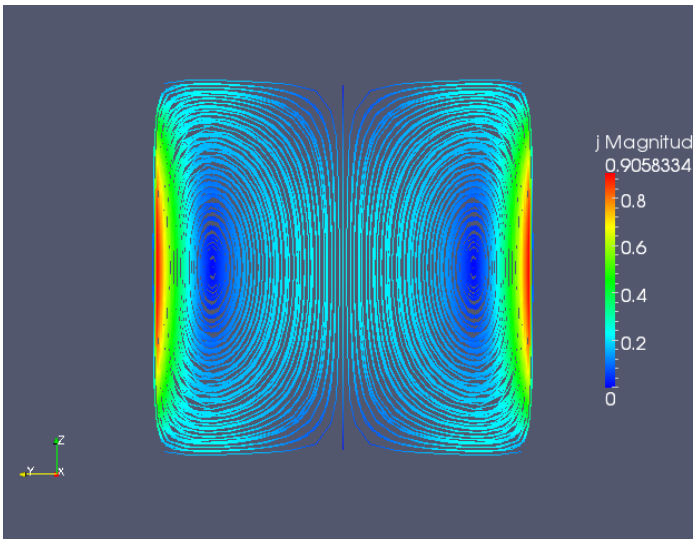

Figure 4.19: 3D MHD pipe flow simulation current density stream lines Hartmann number 10

Following are the results for hartmann number 100. It can be observed that velocity profile for both hartmann layer and side layer are flatter compared to hartmann number 10, as expected.
From looking at current stream lines, it should be noted that compared to hartmann number 10, stream lines are needed to take steep turn near boundaries. The need of conservative[11] scheme becomes more important here. If we take a closer look at side layer velocity profile. Two kinks can be observed. This can be explained by understanding case of hunt's problem (square duct with conductive walls). In hunt[9] problem analytical solution two kinks are observed, very much similar to our case, but a lot bigger. It can be deducted that, due to highly non uniform mesh, some amount of current is able to get into the walls, although we have applied zero normal gradient boundary condition for electric potential at walls. This current causes these kinks just like in the hunt's problem. Although kink is very much small here, it can grow for higher hartmann numbers. All the other results, are very similar to analytical results
.

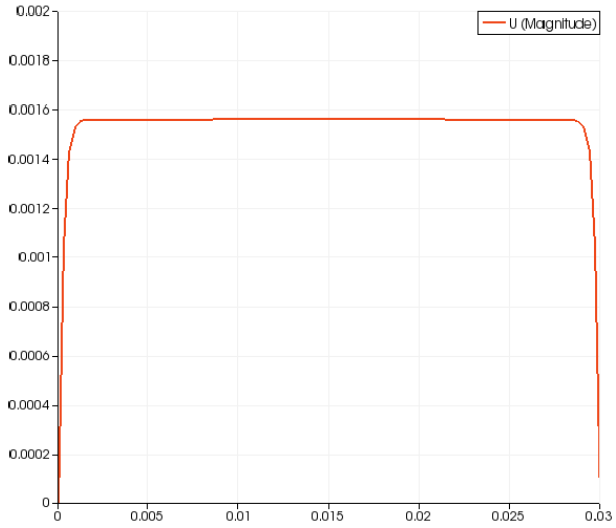

Figure 4.20: 3D MHD pipe flow simulation hartmann layer velocity profile Hartmann number 100

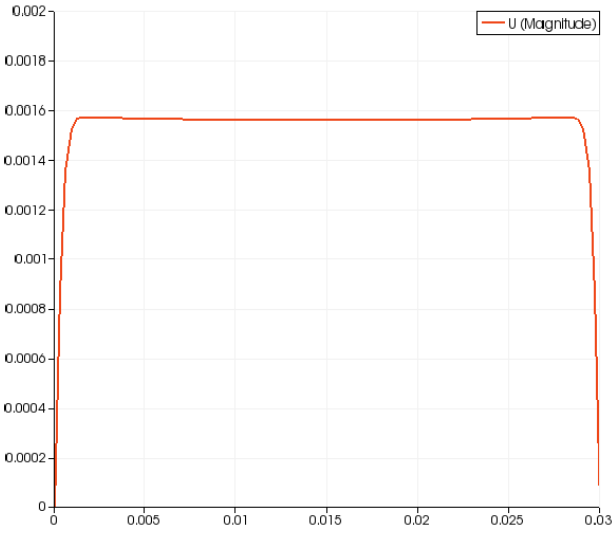

Figure 4.21: 3D MHD pipe flow simulation side layer velocity profile Hartmann number 100

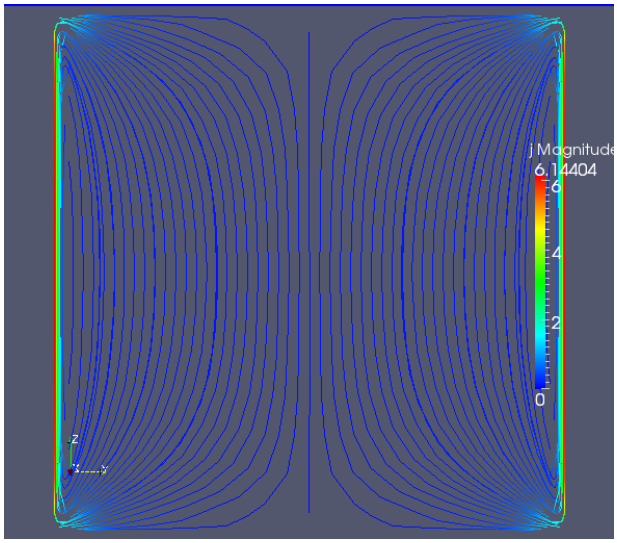

Figure 4.22: 3D MHD pipe flow simulation current density stream lines Hartmann number 100

Now results are presented for hartmann number 500. It can be observed that, here profile is very much flat. By looking at the side layer profile we can say that, kinks are much bigger than hartmann number 100 case. Same explanation can be given here also.

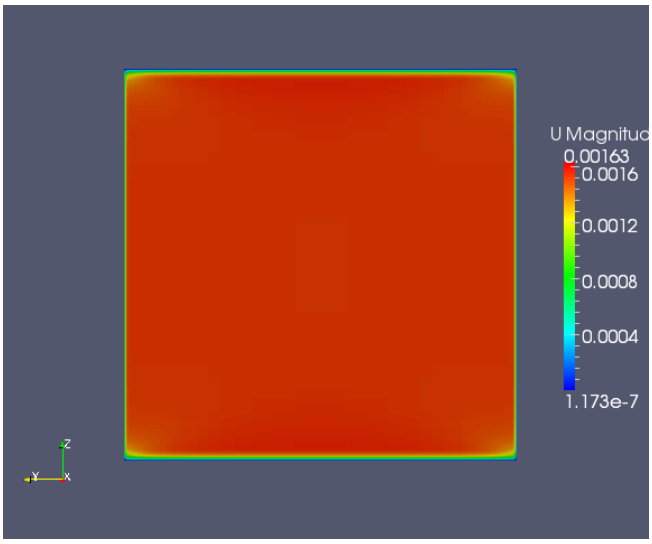

Figure 4.23: 3D MHD pipe flow simulation velocity contour Hartmann number 500

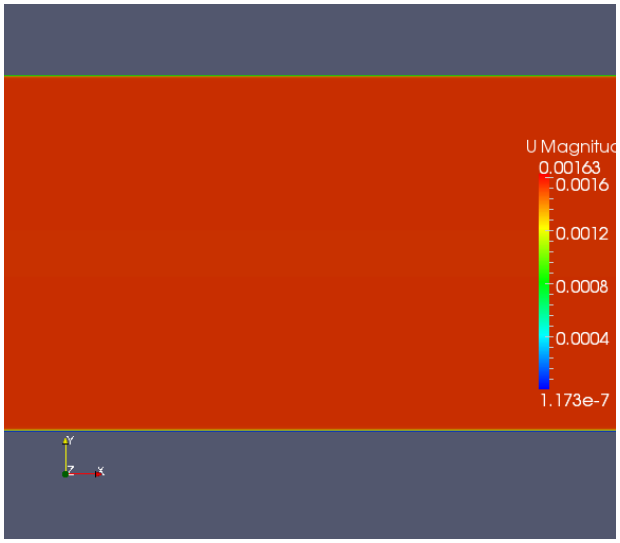

Figure 4.24: 3D MHD pipe flow simulation hartmann layer velocity Hartmann number 500

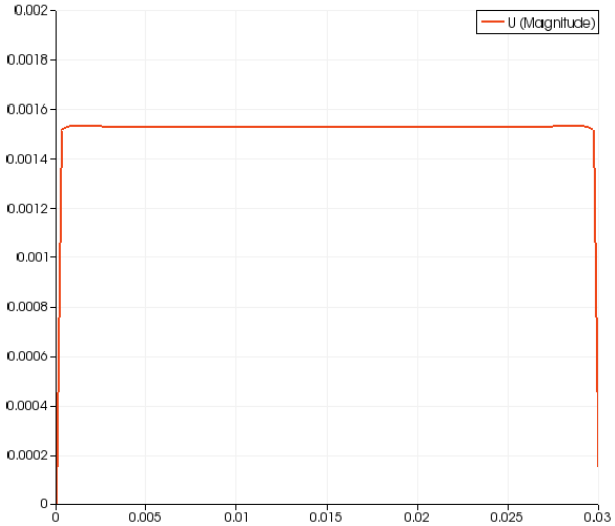

Figure 4.25: 3D MHD pipe flow simulation hartmann layer velocity profile Hartmann number 500

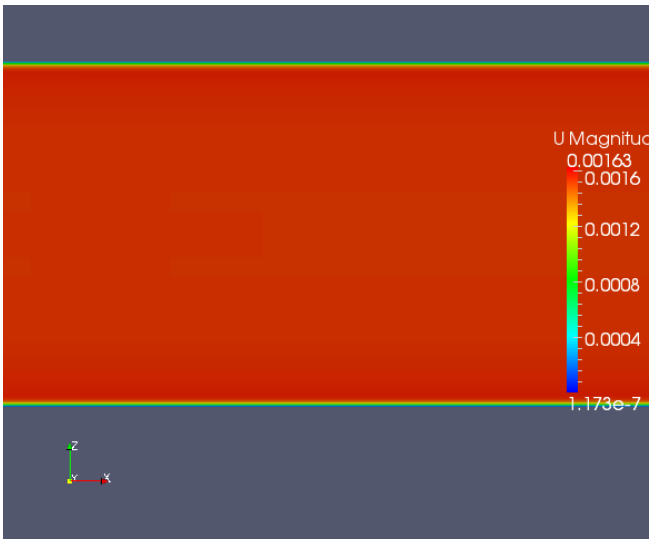

Figure 4.26: 3D MHD pipe flow simulation side layer velocity Hartmann number 500

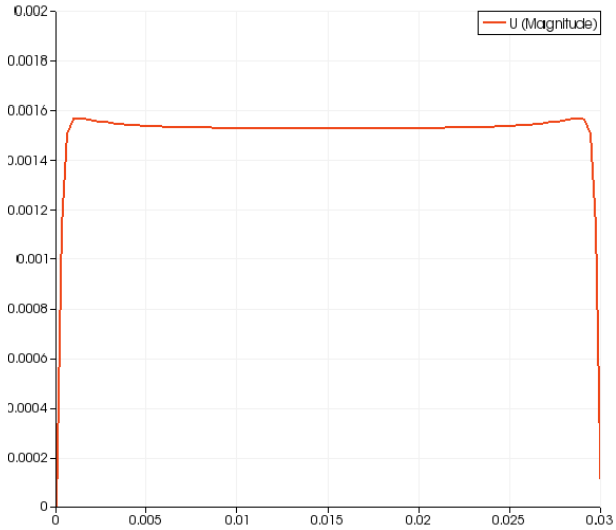

Figure 4.27: 3D MHD pipe flow simulation side layer velocity profile Hartmann number 500

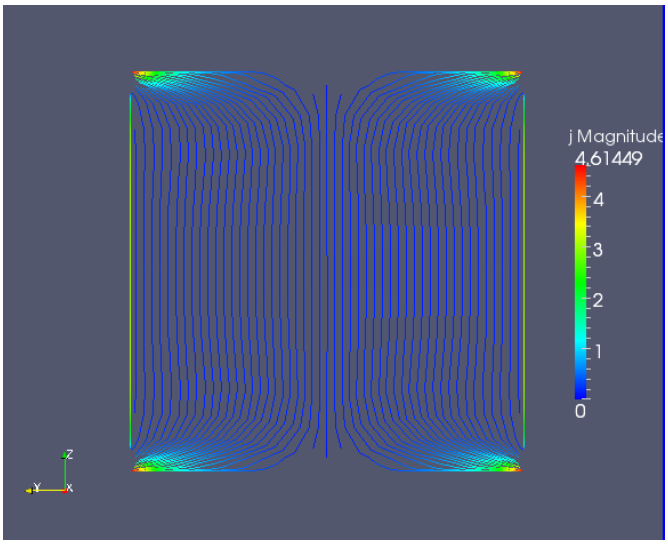

Figure 4.28: 3D MHD pipe flow simulation current density stream lines Hartmann number 500

Simulation is also done for hartmann number 1000 case, where boundary layer is very much thin. Results are presneted in the following figures.

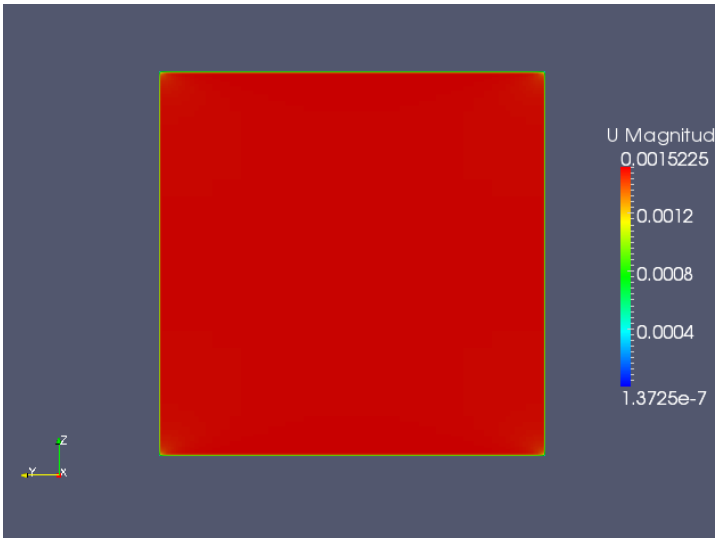

Figure 4.29: 3D MHD pipe flow simulation velocity contour Hartmann number 1000

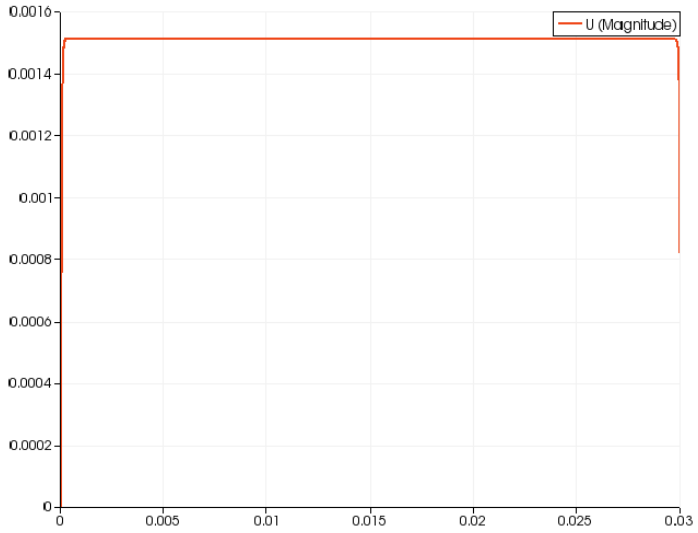

Figure 4.30: 3D MHD pipe flow simulation hartmann layer velocity profile Hartmann number 1000

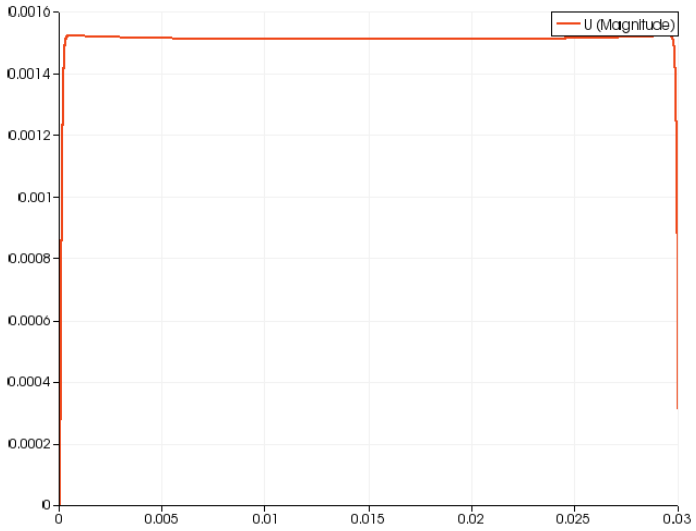

Figure 4.31: 3D MHD pipe flow simulation side layer velocity profile Hartmann number

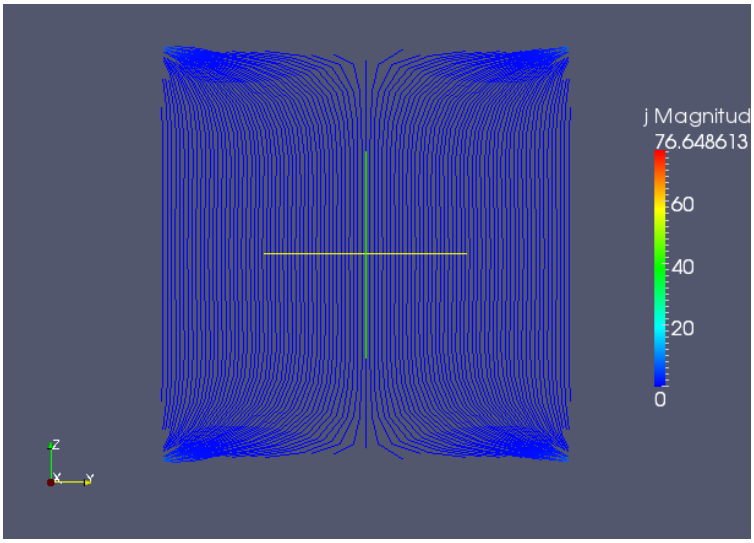

Figure 4.32: 3D MHD pipe flow simulation current density stream lines Hartmann number 1000

The same solver that we have used here also can be used for conductive walls(Hunt case). The only difference will be in boundary condition of electric potential, it should be a constant value instead of zero normal gradient. However for arbitary conductivity material some changes in the solver will be required.

5 Forced Convection for Lead Bismuth Eutectic

In this section a BARC Lead Bismuth Eutectic experimental results[2] are compared with results we get with simulation. BARC has presented their natural convection experimental results for LBE flow in a loop. For some of their results models are created and, transient forced convection simulations are done, to validate them.
There are certain benifits of using LBE over liquid lithium. The high boiling point (1670 C) of LBE ensures that the coolant can be operated at high temperatures without the risk of coolant boiling, which improves the thermal efficiency. It also improves the plant safety by reducing the risk of leakage at high temperatures as pressurization is not required. Also, LBE does not react readily with air or water, and thus, an intermediate coolant is not essential in the reactor. LBE systems are also excellent choices as spallation targets for Accelerator Driven Systems (ADS).

5.1 Case details

The figure 5.1 shows case that is to be simulated. It is a square loop arrangement, red part is the heated section, and blue part is heat exchanger section, where heat will be taken out from liquid metal. The flow in this square loop will be generated by natural convection, very similar to the case of square cavity with one wall hot and another cold.
All the pipes are of circular cross section.

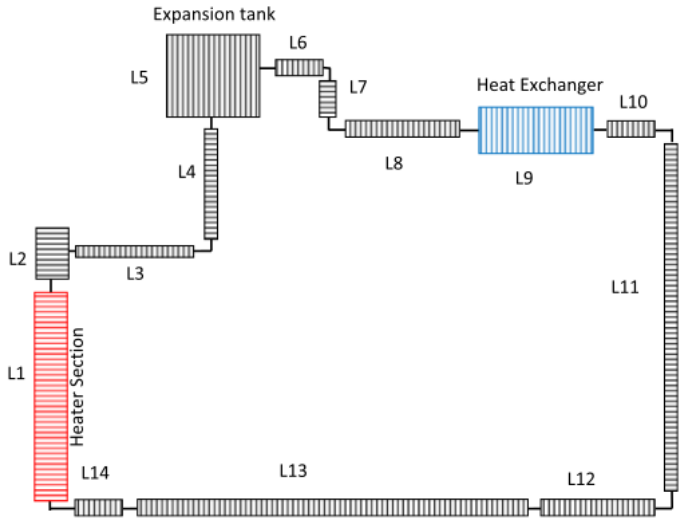

Figure 5.1: LBE BARC test case

The figure 5.2 shows their experimental and simulated results for heated and heat exchanger part.

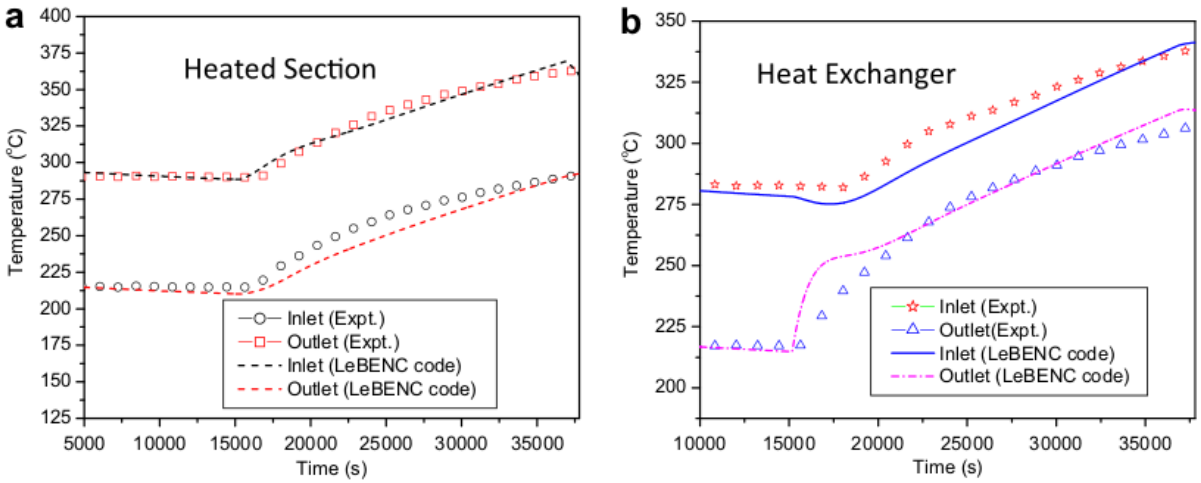

Figure 5.2: LBE BARC experimental temperature profiles

These results represents a situation as following. At start the system is at steday state. 1200 W energy is supplied to the heated section, and the same amount of heat is taken out of heat exchanger section. So, there are no variations with time, but inlet and outlet temperatures for both heated and heat exchanger section are constant. Some temperature loss is happening during the other parts of loop also.

In this steady state region
Heated section: $T_{inlet} = 213^0C$
Heated section: $T_{outlet} = 291^0C$
Heat exchanger section: $T_{inlet} = 282^0C$
Heat exchanger section: $T_{outlet} = 216^0C$

We can observe that in heated section temperature rise is 78_0C and in heat exchanger section temperature loss is 66_0C and thus12_0C is loss in other walls.
Now at $t = 15000s$ the heat exchanger stops working. So, temperature at every point in the loop starts to rise, since more heat is getting in compared to heat getting out. Although heat exchanger stops working, some heat is still coming out of that section, causing some temperature loss in that section.

Heated section: $\Delta T_{heated} = 74^0C$
Heat exchanger section: $\Delta T_{heatexchanger} = 27^0C$

It can be seen that, temperature difference between inlet and outlet nearly stays the same for heated section, since heater input is constant. However, temperature difference across heat exchanger section is quite low compared to steady state.
Slopes for all the four graphs, heated inlet, heated outlet, heat exchanger inlet and heat exchanger outlet are same. The reason for this being, constant net heat supply in the loop.
$Slope = 0.01^0C/s$ Time when change occurs are as following.

Heated section inlet: t=15671 s
Heated section outlet: t=16828 s
Heat exchanger inlet: t=18035 s
Heat exchanger outlet: t=15697 s

Following are the properties experimental setup:

Length of heated section = 800 mm
Diameter of heated section = 80 mm

Length of heat exchanger section = 800 mm
Diameter of heat exchanger section = 80 mm
Total circulation length = 5500 mm
Mass flow rate = 0.09-0.15 kg/s

Following are the thermal properties for Lead Bismuth Eutectic used[1]:

Laminar viscosity = ν = 0.000000192
Thermal expansion coefficient = β = 0.000127
Laminar Prandtl number = Pr = 0.0245
k = 12 W/m/K

It should be noted that this forced convection is different compared to previous simulations, for one this is a transient case, and another that here boundary heat fluc is specified rather than, boundary temperature.

5.2 Numerical Method

Forced convection is studied here.
In this report, two types of simulations are done. For the heated part, since the heat input is known, inlet temperature variation with time is given as a time varying boundary condition, from the experimental result and outlet temperature profile is observed.
For the heat exchanger part, its outlet temperature is given to its inlet with some temp value increased, and a some delay as time varying boundary condition. And inlet and outlet temperature variation are studied.
Mesh used here is like a slice of a cylinder. 6 faced mesh elements are used. In simulations, advantage of axi symmetry is taken. Parabolic velocity profile is specified, and no slip boundary conditions are given at wall. Temperature gradient is specified at walls, in order to apply a specific heat flux.

5.2.1 Modelling

Heated part

For this part, time varying inlet temperature profile is given. We can comment the following:

$|T_{outlet} - T_{Inlet}| \propto \frac{dT}{dx} \times Area$

$k\frac{dT}{dx}$ =heat flux per unit area

Although the inlet profile as in the experimental result is not exactly straight line, in this case, it is considered to be a straight line.
Heat exchanger part

As discussed in previous sections, some things to be modeled here are as following:
Delay time
Temp increase
Heat flux out of heat exchanger part after failure
Temperature boundary condition for heat exchanger inlet is constant temperature for some initial time (steady state), and after that :

$T_{inlet}(t) = T_{outlet}(t - tdelay) + T_{increment}$

Rayleigh number for this case turns out to be of the order to 10^7 which is quite high, suggesting ,

most of the temperature transport is happening through convection only.

Estimation of heat flux out of heat exchanger part after failure

This is done by two methods. One by using $|T_{outlet} - T_{Inlet}|$ from experimental data, and relating it to heat flux through heat exchanger wall.
One thing we can tell from the straight line between temperature and time is; heat flux out of heat exchanger remains constant after some time. Now from the slope of this straight line, heat getting inside this system per unit time is calculated from experimental result using total volume of the fluid in whole system, and from that and heated part heat flux, heat exchanger flux is estimated.
These methods give a little bit different result from one another, but when various cases were simulated, it turned out that first method is more useful.

Temp increase
This value is selected on basis of heated part simulations. Since nothing has changed for the heated part and other parts of loop temperature increae, is taken as temperature increase in heated part minus, loss in other regions.

Delay time

Rayleigh number for this case turns out to be of the order to 10^7 which is quite high, suggesting , most of the temperature transport is happening through convection only.
Times from experimental results does not seem much useful for this modelling. Since major heat transfer is using convection, time in which the flow completes one circle of the loop, can be taken as delay time.
However it was noticed that, the same thing can be done by for given, heat flux, and temperature increment, by varying delay time, to get expected temperature-time slope.

In summary, heat flux from heat exchanger is estimated from $|T_{outlet} - T_{Inlet}|$ experimental result. Temperature increment is estimated from heated part simulations and experimental results. Delay time is estimated from total time to complete one loop for flow, and fine adjustments are done by fixing heat flux, and temperature increment and varying delay time in order to get experimented temperature-time slope.
Folliwing are the parameters used in simulations:
Delay = 2700 s
Temperature increase = 78 K

5.2.2 Simulation

Since this is transient simulation, instead of SIMPLE method, where relaxation factor is used, PISO method is used. OpenFOAM buoyantBoussinisqPimpleFoam solver is used.
In order to provide time varying boundary conditions, groovyBC is used. funkySetFields is used to set initial conditions.

5.3 Results

5.3.1 Heated region

We can easily see that simulation results are very similar to experimental results. Parameters to compare are $|T_{outlet} - T_{Inlet}|$ and temperature-time slope.

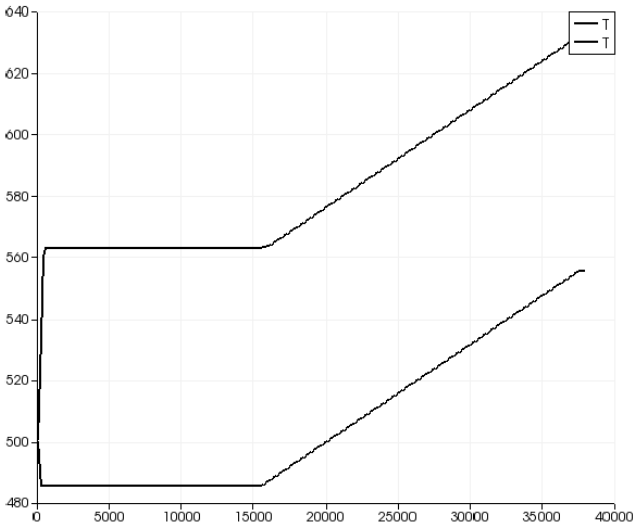

Figure 5.3: LBE BARC simulated for heated part

5.3.2 Heat exchanger

When above calculated modelling parameters are used, following profiles are obtained. Profiles are coming out to be oscillating instead of a straight line.
The above phenomenon can be explained as following:
When a step is given in the heat flux coming out of heat exchanger, the time scale for that change happening is much smaller compared to our delay time. Which causes these oscillations, which eventually die out, as time proceeds.

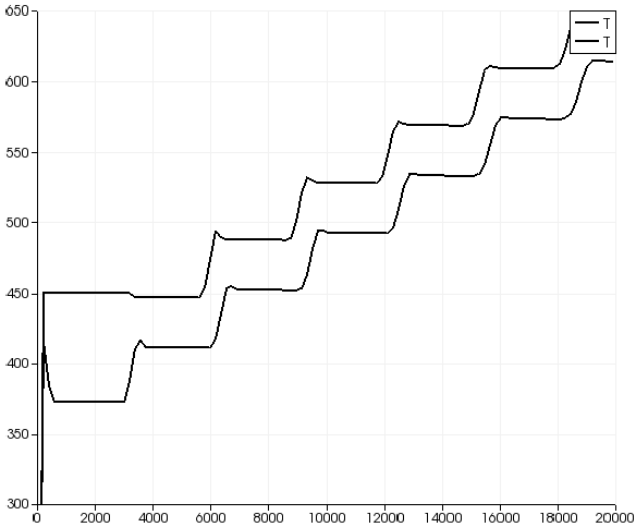

Figure 5.4: Heat exchanger simulation with delay and step heat flux

In order to improve this, instead of a step increase in heat flux, a ramp increase is given, with time scale comparable to delay time. This works well and we get the following profile.

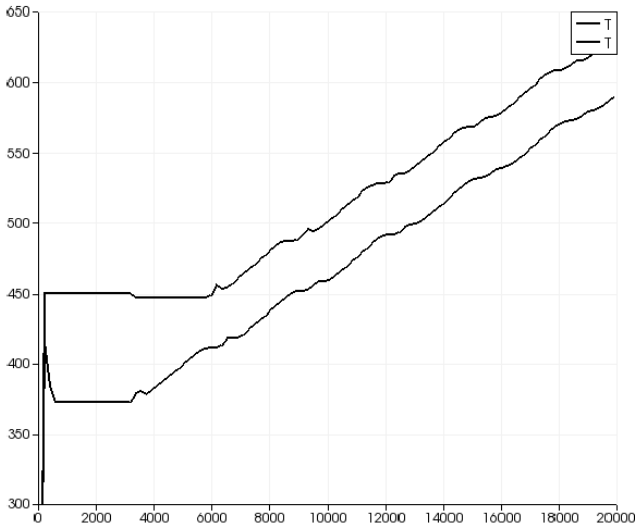

Figure 5.5: Heat exchanger simulation with delay and ramp heat flux

Again, $|T_{outlet} - T_{Inlet}|$ and temperature-time slope can be compared with experimental results. But still in this result also we are getting a kink. That again comes out due to modelling error. It can be argued that, this is like a overshoot in the system, and it has nothing to do with delay, since this appears before the first delay loop for outlet.

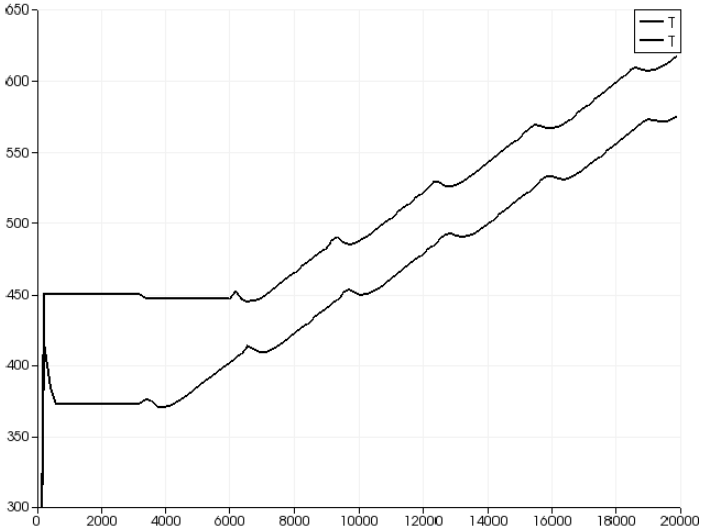

Figure 5.6: Heat exchanger simulation with delay and two ramps heat flux

From this observation, need arises to model the heat flux profile properly. It seems that, in the initial region slope of profile should be lower, and in later region it should be more. Applying this gives the following profile. This profile matches quite nicely, but still scope remains for modifications.

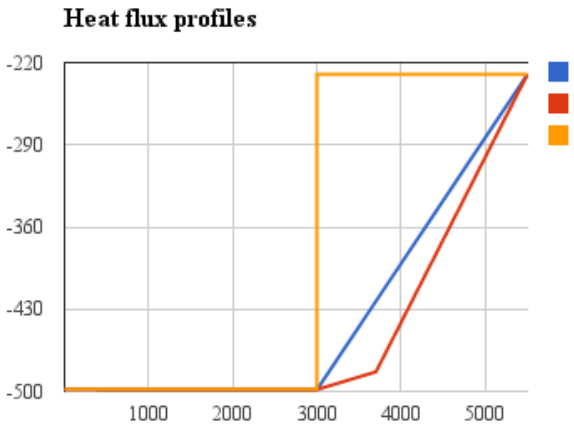

Figure 5.7: Various heat flux profiles used for simulation

Thus we conclude that, heat flux profile modelling turns out to be very important parameter.

6 Conclusion

- Forced convection results are extended to natural convetion. Natural convection simulations are done for cavity and open pipe cases.
- A new fast converging, solver is created using electric potential method for MHD problems.
- Using the new solver 2D and 3D MHD cases are simulated.
- And in the last, a BARC LBE heater - heat exchanger loop experimental results are compared with simulated results.
  Still, combining heat transfer and MHD solvers is left, which is the main goal of this project.

Appendices

MHD solver electric potential method

```
    Info<< nl << "Starting time loop" << endl;

    while (runTime.loop())
    {
        #include "readPISOControls.H"
        #include "readBPISOControls.H"

        Info<< "Time = " << runTime.timeName() << nl << endl;
        Info<< "ExecutionTime = " << runTime.elapsedCpuTime() << " s"<< " ClockTime = " <<
            runTime.elapsedClockTime() << " s"<< nl << endl;

        #include "CourantNo.H"

        {
            volVectorField UcrosB= U ^ B;
            j=-sigma*fvc::grad(epo) + sigma*UcrosB;
            volVectorField jcrosB = j ^ B;
            fvVectorMatrix UEqn
            (
                fvm::ddt(U)
              + fvm::div(phi, U)
              - (jcrosB/rho)
              - fvm::laplacian(nu, U)
            );
            UEqn.relax();
            solve(UEqn == -fvc::grad(p));


            // --- PISO loop

            for (int corr=0; corr<nCorr; corr++)
            {
                p.storePrevIter();
                volScalarField rAU(1.0/UEqn.A());

                U = rAU*UEqn.H();

                phi = (fvc::interpolate(U) & mesh.Sf())
                    + fvc::ddtPhiCorr(rAU, U, phi);

                for (int nonOrth=0; nonOrth<=nNonOrthCorr; nonOrth++)
                {
                    fvScalarMatrix pEqn
                    (
                        fvm::laplacian(rAU, p) == fvc::div(phi)
                    );

                    pEqn.setReference(pRefCell, pRefValue);
                    pEqn.solve();

                    if (nonOrth == nNonOrthCorr)
                    {
                        phi -= pEqn.flux();
                    }
                p.relax();
                }
```

```
            #include "continuityErrs.H"

            U -= rAU*fvc::grad(p);
            U.correctBoundaryConditions();
        }
    }

    // --- B-PISO loop

    for (int Bcorr=0; Bcorr<nBcorr; Bcorr++)
    {
        volVectorField UcrosB= U ^ B;
        fvScalarMatrix BEqn
        (
            fvm::laplacian(epo) - fvc::div(UcrosB)
        );

        BEqn.solve();

        // #include "magneticFieldErr.H"
    }

    runTime.write();
}

Info<< "End\n" << endl;

return 0;
}
```

References

[1] *Handbook on Lead-bismuth Eutectic Alloy and Lead Properties, Materials, Compatibility, Thermal-hydraulics and Technologies.*

[2] N.K. Maheshwari P.K. Vijayan D. Saha R.K. Sinha A. Borgohain, B.K. Jaiswal. Natural circulation studies in a lead bismuth eutectic loop. *Progress in nuclear energy*, 53:308–319, 2011.

[3] Adrian Bejan. *Convective Heat Transfer*. John Wiley and sons, 2004.

[4] Herman Branover. *Magnetohydrodynamic flow in ducts*. John Wiley and sons, 1978.

[5] A. Bhattarchjee D. A. Gurnett. *Introduction to Plasma Physics*. Cambridge university press, 2005.

[6] L. F. A. Azevedo E. M. Sparrow. Vertical - channel natural convection spanning between the fully - developed limit and the single -plate boundaey - layer limit. *International Journal of Heat and Mass transfer*, 28:1847–1857, 1985.

[7] L. Batet I. Ricapito A. Aiello O. Gastaldi F. Gabriel E. Mas de les Valls, L.A. Sedano. Lead–lithium eutectic material database for nuclear fusion technology. *Journal of nuclear materials*, 376:353–357, 2008.

[8] L. Bateta c V. de Medinaa d J. Fraderaa c E.Mas de les Valls a, b and L. Sedanoe. Modelling of integrated effect of volumetric heating and magnetic field on tritium transport in a u-bend flow as applied to hcll blanket concept. *Fusion engineering and design*, 86:341–356, 2011.

[9] J. C. R. Hunt. Magnetohydrodynamics flow in rectengular ducts. *Journal of Fluid Mechanics*, 21:577–590, 1965.

[10] L. Leboucher. Monotone Scheme and Boundary Conditions for Finite Volume Simulation of Magnetohydrodynamic Internal Flows at High Hartmann Number . Centre for Numerical Modelling and Process Analysis, University of Greenwich, London SE18 6PF, United Kingdom, November 1998.

[11] Neil B. Morley Peter Huang Mohamed A. Abdou Ming-Jiu Ni, Ramakanth Munipalli. A current density conservative scheme for incompressible mhd flows at a low magnetic reynolds number. part i: On a rectangular collocated grid system. *Journal of Computational Physics*, 227:174–204, 2007.

[12] J. A. Shercliff. Steady motion of conducting fluids in pipes under transverse magnetic fields. 1952.